# Do Polyepoxy/Polyisocyanate Composite Resins for Concrete Protection Perform Better Than Either of Their Components?

Stefan H. Bossmann, Ph.D.
Madumali Kalubowilage, Ph.D.

*Kansas State University*

Kansas
Department of Transportation

| 1 | Report No. KS-20-01 | 2 | Government Accession No. | 3 | Recipient Catalog No. |
|---|---|---|---|---|---|
| 4 | Title and Subtitle<br>Do Polyepoxy/Polyisocyanate Composite Resins for Concrete Protection Perform Better Than Either of Their Components? | | | 5 | Report Date<br>January 2020 |
| | | | | 6 | Performing Organization Code |
| 7 | Author(s)<br>Stefan H. Bossmann, Ph.D., Madumali Kalubowilage, Ph.D. | | | 8 | Performing Organization Report No. |
| 9 | Performing Organization Name and Address<br>Kansas State University<br>Department of Chemistry<br>213 CBC Building<br>1212 Mid-Campus Drive North<br>Manhattan, KS 66506-0401 | | | 10 | Work Unit No. (TRAIS) |
| | | | | 11 | Contract or Grant No.<br>C2119 |
| 12 | Sponsoring Agency Name and Address<br>Kansas Department of Transportation<br>Bureau of Research<br>2300 SW Van Buren<br>Topeka, Kansas 66611-1195 | | | 13 | Type of Report and Period Covered<br>Final Report<br>January 2018–March 2019 |
| | | | | 14 | Sponsoring Agency Code<br>RE-0744-01 |

| 15 | Supplementary Notes<br>For more information write to address in block 9. |
|---|---|

**16  Abstract**

Polyepoxy and polyisocyanate resins are currently in use for protecting concrete and especially steel structural elements in concrete from water-induced corrosive processes. The newest class of materials consists of polyepoxy/polyisocyanate composite resins. The underlying paradigm of using these composite materials is that they show structural synergy, leading to improved material properties, such as improved adhesion to concrete surfaces and higher durability, resilience, and weather resistance.

The first phase of this research project consisted of the synthesis and chemical characterization of the required polyisocyanate resins and polyepoxy/amine resins. These resins are required, because their interaction with each other when adsorbed on concrete will be studied in Phase 2. The research team then investigated the chemical interaction between the model resins that were optimized in the first phase of this project in Phase 2. The thermal stabilities of the resulting composite materials were studied to estimate their resistance against weathering. Researchers could observe enhanced stability of polyisocyanate/polyepoxy/amine co-resins at very broad mixing ratios (5:95 to 95:5 weight ratios), with a maximum of thermal stability at 75:25 polyisocyanate to polyepoxy resin precursors. The observed increase in thermal stability was attributed to the formation of urea-type bonds between isocyanates and amines. This reaction can only occur if the resin precursors for polyisocyanates and polyepoxy/amines are mixed. This formation of novel bonds has been corroborated by nuclear magnetic resonance ($^1$H-NMR) spectroscopy. The third phase of this research project consisted of the atomic force microscopy (AFM) and magnetic resonance imaging (MRI) of two types of wafers that were provided by KDOT, as well as coated wafers. The final phase of this research project consisted of MRI of optimized polyepoxyamine resin (B) on the surfaces of Type 2 concrete model wafers provided by KDOT.

FLASH, RARE, and Turbo-RARE imaging clearly demonstrated that polyepoxyamine resin (B) is a very suitable polymer coating for Type 2 concrete wafers. This proves that ultra-high-field MRI imaging is an excellent method for imaging polymer-concrete interfaces. The results clearly demonstrate that polyepoxyamine resins are, principally, superior as protective concrete coatings to polyurethane coatings, which were found not to be strongly adhesive. Mixtures of polyepoxyamine and polyurethane resins were dominated by their polyurethane content and, therefore, not as suitable as pure polyepoxyamine resins.

| 17 | Key Words<br>Protective Coating, Composite Materials, Resins, Adhesion | 18 | Distribution Statement<br>No restrictions. This document is available to the public through the National Technical Information Service www.ntis.gov. |
|---|---|---|---|
| 19 | Security Classification (of this report)<br>Unclassified | 20  Security Classification (of this page)<br>Unclassified | 21  No. of pages<br>72 | 22  Price |

Form DOT F 1700.7 (8-72)

This page intentionally left blank.

# Do Polyepoxy/Polyisocyanate Composite Resins for Concrete Protection Perform Better Than Either of their Components?

Final Report

Prepared by

Stefan H. Bossmann, Ph.D.
Madumali Kalubowilage, Ph.D.

Kansas State University

A Report on Research Sponsored by

January 2020

# NOTICE

The authors and the state of Kansas do not endorse products or manufacturers. Trade and manufacturers names appear herein solely because they are considered essential to the object of this report.

This information is available in alternative accessible formats. To obtain an alternative format, contact the Office of Public Affairs, Kansas Department of Transportation, 700 SW Harrison, 2nd Floor – West Wing, Topeka, Kansas 66603-3745 or phone (785) 296-3585 (Voice) (TDD).

# DISCLAIMER

The contents of this report reflect the views of the authors who are responsible for the facts and accuracy of the data presented herein. The contents do not necessarily reflect the views or the policies of the state of Kansas. This report does not constitute a standard, specification or regulation.

# Abstract

Polyepoxy and polyisocyanate resins are currently in use for protecting concrete and especially steel structural elements in concrete from water-induced corrosive processes. The newest class of materials consists of polyepoxy/polyisocyanate composite resins. The underlying paradigm of using these composite materials is that they show structural synergy, leading to improved material properties, such as improved adhesion to concrete surfaces and higher durability, resilience, and weather resistance.

The first phase of this research project consisted of the synthesis and chemical characterization of the required polyisocyanate resins and polyepoxy/amine resins. These resins are required, because their interaction with each other when adsorbed on concrete will be studied in Phase 2. The research team then investigated the chemical interaction between the model resins that were optimized in the first phase of this project in Phase 2. The thermal stabilities of the resulting composite materials were studied to estimate their resistance against weathering. Researchers could observe enhanced stability of polyisocyanate/polyepoxy/amine co-resins at very broad mixing ratios (5:95 to 95:5 weight ratios), with a maximum of thermal stability at 75:25 polyisocyanate to polyepoxy resin precursors. The observed increase in thermal stability was attributed to the formation of urea-type bonds between isocyanates and amines. This reaction can only occur if the resin precursors for polyisocyanates and polyepoxy/amines are mixed. This formation of novel bonds has been corroborated by nuclear magnetic resonance ($^1$H-NMR) spectroscopy. The third phase of this research project consisted of the atomic force microscopy (AFM) and magnetic resonance imaging (MRI) of two types of wafers that were provided by KDOT, as well as coated wafers. The final phase of this research project consisted of MRI of optimized polyepoxyamine resin (B) on the surfaces of Type 2 concrete model wafers provided by KDOT.

FLASH, RARE, and Turbo-RARE imaging clearly demonstrated that polyepoxyamine resin (B) is a very suitable polymer coating for Type 2 concrete wafers. This proves that ultra-high-field MRI imaging is an excellent method for imaging polymer-concrete interfaces. The results clearly demonstrate that polyepoxyamine resins are, principally, superior as protective concrete coatings to polyurethane coatings, which were found not to be strongly adhesive. Mixtures of polyepoxyamine and polyurethane resins were dominated by their polyurethane content and, therefore, not as suitable as pure polyepoxyamine resins.

# Acknowledgements

# Table of Contents

# List of Tables

# List of Figures

# Chapter 1: Introduction

## 1.1 Overview

Polyepoxy and polyisocyanate resins are currently in use for protecting concrete and especially steel structural elements in concrete from water-induced corrosive processes. The newest class of materials consists of polyepoxy/polyisocyanate composite resins. The underlying paradigm of using these composite materials is that they show structural synergy, leading to improved material properties, such as improved adhesion to concrete surfaces and higher durability, resilience, and weather resistance.

## 1.2 Background

Before the beginning of this study, no systematic data was available describing the interactions of polyepoxy/polyisocyanate composite resins, as well as their behavior on concrete wafers. Furthermore, no suitable literature on the synthesis of model concrete wafers, and the requirements for suitable concrete wafers for MRI studies of polymer resin adhesion, could be found.

## 1.3 Problem Statement

This project aims to study the interaction mechanisms of polyepoxy/polyisocyanate composite resins in comparison with polyepoxy resins and polyisocyanate resins utilizing established methods in polymer science and surface characterization.

## 1.4 Objectives

The proposed study has the following specific objectives:

1. Synthesis and characterization of polyisocyanate resins from VORANOL 220-110 (DOW) and mixtures of TDI (toluene, diisocyanates) and MDI (methylene diphenyl diisocyanate).
   a. Study of chemical composition by means of Fourier-transform infrared spectroscopy (FTIR) and nuclear magnetic resonance ($^1$H and $^{13}$C-NMR).

b.  Study of the physical and chemical properties of polyisocyanate resin films on surfaces (mica and model concrete) by means of atomic force microscopy (AFM): surface roughness and recognition of polymer domains on the surface; FTIR: reaction kinetics of film formation; reflection electron microscopy (REM): surface topology; and ultra-high field magnetic resonance imaging (MRI): formation of polymer domains and polymer adhesion to concrete surfaces.

2.  Chemical and physical characterization of polyepoxy resins (D.E.R. 325 or D.E.R. 3401; Olin Corporation, 2019b).

a.  Study of chemical composition by means of Fourier-transform infrared spectroscopy (FTIR) and nuclear magnetic resonance ($^1$H and $^{13}$C-NMR).

b.  Study of the physical and chemical properties of polyepoxy resin films on surfaces (mica and model concrete) by means of atomic force microscopy (AFM): surface roughness and recognition of polymer domains on the surface; FTIR: reaction kinetics of film formation; reflection electron microscopy (REM): surface topology; and ultra-high field magnetic resonance imaging (MRI): formation of polymer domains and polymer adhesion to concrete surfaces.

3.  Synthesis and Characterization of mixtures of polyisocyanate and polyepoxy resins

a.  Study of chemical composition by means of Fourier-transform infrared spectroscopy (FTIR) and nuclear magnetic resonance ($^1$H and $^{13}$C-NMR).

b.  Study of the physical and chemical properties of composite resin films on surfaces (mica and model concrete) by means of atomic force microscopy (AFM): surface roughness and recognition of polymer domains on the surface; FTIR: reaction kinetics of film formation; reflection electron microscopy (REM): surface topology; and ultra-

high field magnetic resonance imaging (MRI): formation of polymer domains and polymer adhesion to concrete surfaces.

## 1.5 Scope

The scope of the proposed study is to prove or disprove the existence of polyepoxy/polyisocyanate composite domain with enhanced material properties. Comparing the results from Objectives (1) and (2) with the spectral/imaging information that will be obtained in Objective (3) will enable the research team to discover the extent and the mechanisms in favor of polymer-polymer interaction. This will enable researchers to make predictions about the usefulness of the resins for the purpose of corrosion protection of concrete.

# Chapter 2: Synthesis and Characterization of Polyisocyanate Resins from VORANOL 220-110 (DOW) and Mixtures of TDI (Toluene, Diisocyanates) and MDI (Methylene Diphenyl Diisocyanate)

## 2.1 Polyisocyanate Resins from VORANOL 220-110 (DOW) and TDI (Toluene, Diisocyanates)

VORANOL 220-110 is a polyether polyol homopolymer (molecular weight ~1000 g/mole), derived from propylene oxide. It contains two terminal hydroxyl groups, which react with the isocyanate groups of ortho-, para-toluene diisocyanate (93%, shown) and ortho-, ortho- toluene diisocyanate (6%, not shown) to linear polyurethane chains and then polyurethane networks (with ortho-, ortho-, para-toluene triisocyanate (TTI), 1%, not shown). The principal reaction between VORANOL 220-110 and TDI is shown in Figure 2.1.



further polymerization and network formation
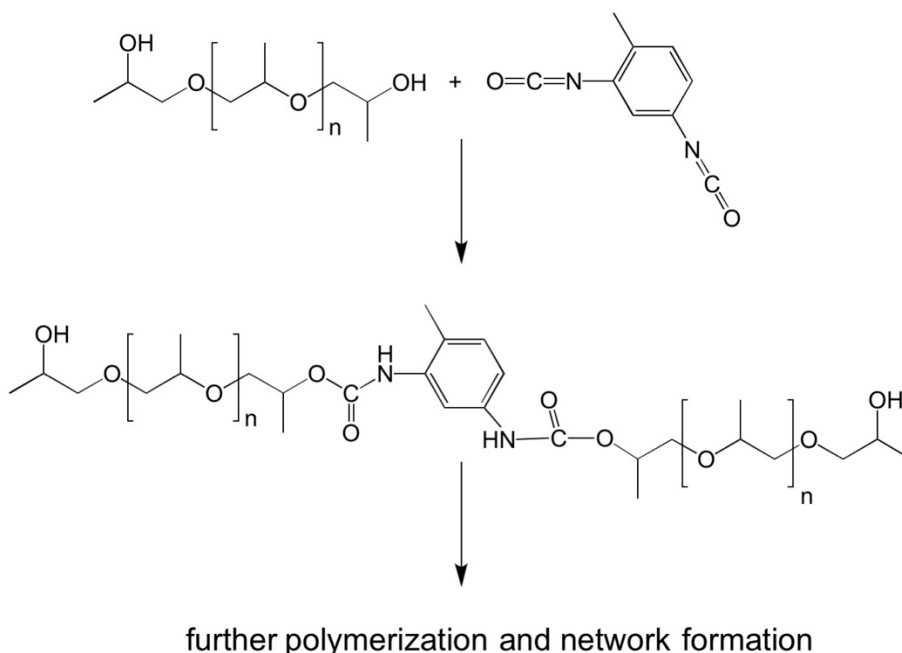
**Figure 2.1: Principal Reactions during the Thermal Crosslinking of VORANOL 220-110 and TDI**
Source: Akindoyo et al. (2016)

A series of five initial polymerization reactions were performed with varying ratios of VORANOL 220-110 to TDI (55:45, 52:48, 50:50, 48:52, 45:55, all ratios are molar ratios) at 25 °C. The initial viscosity of the mixtures ranged from 220 to 280 mPa·s, which agreed with data

provided by Olin Corporation (2019b), a subsidiary of The Dow Chemical Company. In Table 2.1, the initial viscosity, the viscosity after 1 hour, and the threshold of thermal stability, as determined by means of differential thermogravimetry analysis (DTA), are summarized.

**Table 2.1: Investigated Mixtures of VORANOL 220-110 and Toluene Diisocyanate (Technical Mixture Consisting of 93% o,p-TDI, 6% o,o-TDI, and 1% o,o,p-TTI)**

| Test Mixture Number | Molar Ratio of VORANOL 220-100 to TDI | Initial Viscosity (mPa·s) | Viscosity after 60 min. (mPa·s) | Threshold of Thermal Decomposition |
|---|---|---|---|---|
| 0 | 100:0 | 220 | 220 | 250 °C |
| 1 | 55:45 | 240 | 1,300 | 260 °C |
| 2 | 52:48 | 240 | 10,600 | 275 °C |
| 3 | 50:50 | 250 | 45,200 | 320 °C |
| 4 | 48:52 | 280 | > 60,000[*] | 345 °C |
| 5 | 45:55 | 280 | 50,800 | 335 °C |

[*]Maximum of measurable viscosity

**According to the polymerization experiments summarized in Table 2.1, the ratio of 48 mole % VORANOL 210-110 and 52% TDI led to the best polyurethane resin in this series.** This is in agreement with the technical specifications of VORANOL 220-110, which describe 2.2 to 2.3 hydroxyl groups polyether polyol chain (Olin Corporation, 2019b).
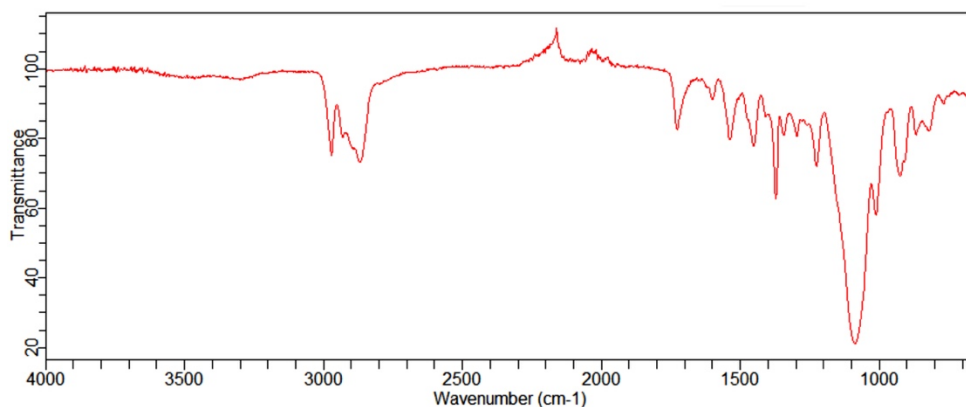


**Figure 2.2: FTIR of test mixture #4 on alumina after 60 minutes of curing reaction.**
The transmission infrared spectrum (peaks go "down") shows peaks at 3250 cm⁻¹, >3000 cm⁻¹, 1730 cm⁻¹, 1610 cm⁻¹, 1510 cm⁻¹, 1450 cm⁻¹, and 1390 cm⁻¹.

In Figure 2.2, the FTIR spectrum of test mixture #4 (Molar Ratio of VORANOL 220-110 to TDI of 48:52) is shown. The absence of a strong hydroxyl peak at 3500 to 3200 cm⁻¹ indicates

a virtually complete reaction of the hydroxyl groups after 60 minutes. A weak amine (NH) peak at 3250 cm$^{-1}$, aromatic CH transitions (> 3000 cm$^{-1}$, 1610 cm$^{-1}$, and 1510 cm$^{-1}$), aliphatic CH transitions (<3000 cm$^{-1}$, 1450 cm$^{-1}$, and 1390 cm$^{-1}$), as well as the signature urethane carbonyl group at 1730 cm$^{-1}$ are clearly discernible.

## 2.2 Polyisocyanate Resins from VORANOL 220-110 (DOW) and MDI (Methylene Diphenyl Diisocyanate)

The principal reaction between VORANOL 220-110 (molecular weight ~1000 g/mole) and methylene diphenyl diisocyanate (MDI) is shown in Figure 2.3. The major difference between MDI and TDI is that the former does not contain a small amount of tri-functional isocyanate. However, as already discussed, VORANOL 220-110 contains 2.2 to 2.3 hydroxyl groups per polyether polyol chain. Therefore, limited crosslinking occurs also with MDI as the data indicates, summarized in Table 2.2.
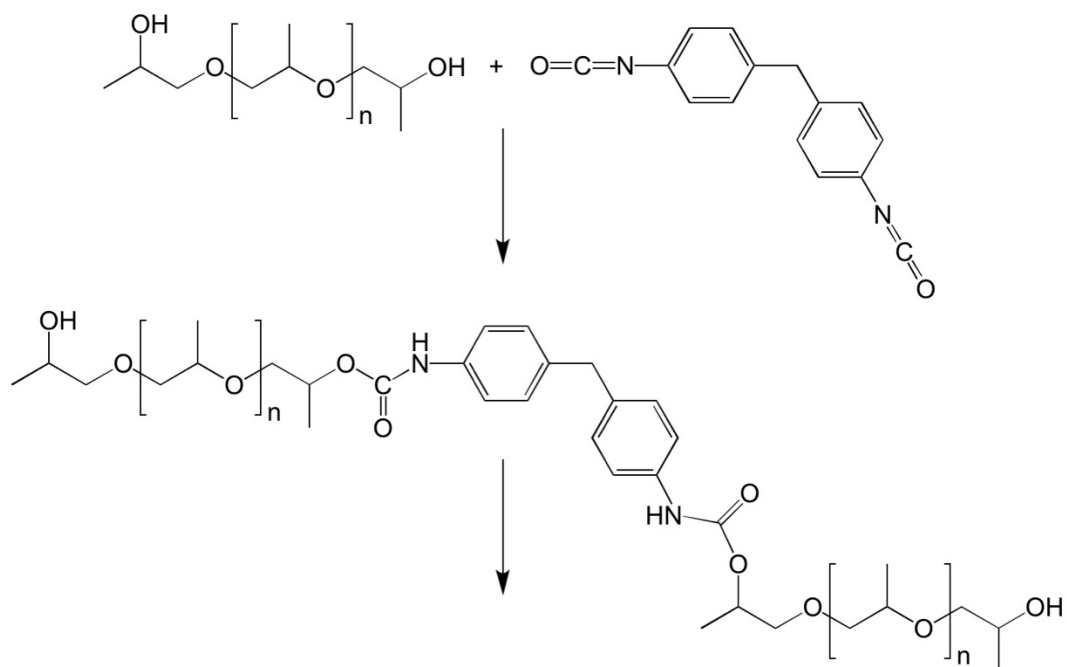


**Figure 2.3: Principal Reactions during the Thermal Crosslinking of VORANOL 220-110 and MDI**
Source: Akindoyo et al. (2016)

A series of five initial polymerization reactions were performed with varying ratios of VORANOL 220-110 to MDI (55:45, 52:48, 50:50, 48:52, 45:55, all ratios are molar ratios) at 25 °C. The initial viscosity of the mixtures ranged from 220 to 400 mPa·s, which was in agreement with data provided by Olin Corporation (2019b). In Table 2.2, the initial viscosity, the viscosity after 1 hour, and the threshold of thermal stability, as determined by means of differential thermogravimetry analysis (DTA), are summarized.

**Table 2.2: Investigated Mixtures of VORANOL 220-110 and Methylene Diphenyl Diisocyanate (MDI)**

| Test Mixture Number | Molar Ratio of VORANOL 220-100 to MDI | Initial Viscosity (mPa·s) | Viscosity after 60 min. (mPa·s) | Threshold of Thermal Decomposition |
|---|---|---|---|---|
| 0 | 100:0 | 220 | 220 | 250 °C |
| 1 | 55:45 | 290 | 2,500 | 285 °C |
| 2 | 52:48 | 300 | 12,000 | 295 °C |
| 3 | 50:50 | 340 | 35,800 | 340 °C |
| 4 | 48:52 | 380 | > 60,000[*] | 365 °C |
| 5 | 45:55 | 400 | > 60,000[*] | 360 °C |

[*]Maximum of measurable viscosity

In agreement with the polymerization experiments summarized in Table 2.2, the ratio of 48 mole% VORANOL 210-110 and 52% MDI led to the best polyurethane resin in this series. This is in agreement with the technical specifications of VORANOL 220-110, which describe 2.2 to 2.3 hydroxyl groups per polyether polyol chain (Olin Corporation, 2019b). In comparison with TDI-derived polyurethane coatings, MDI-derived polyurethanes display a somewhat higher thermal stability, due to the presence of the methylene diphenyl diisocyanate (MDI) group.

**Figure 2.4: FTIR of test mixture #4 on alumina after 60 minutes of curing reaction**
The transmission infrared spectrum (peaks go "down") shows peaks at 3300 cm$^{-1}$, > 3000 cm$^{-1}$, 1725 cm$^{-1}$, 1610 cm$^{-1}$, 1495 cm$^{-1}$, 1450 cm$^{-1}$, and 1390 cm$^{-1}$.

In Figure 2.4, the FTIR spectrum of test mixture #4 (Molar Ratio of VORANOL 220-110 to MDI of 48:52) is shown. The absence of a strong hydroxyl peak at 3500 to 3200 cm$^{-1}$ indicates a virtually complete reaction of the hydroxyl groups after 60 minutes. A weak amine (NH) peak at 3300 cm$^{-1}$, aromatic CH transitions (> 3000 cm$^{-1}$, 1610 cm$^{-1}$, and 1495 cm$^{-1}$), aliphatic CH transitions (<3000 cm$^{-1}$, 1450 cm$^{-1}$, and 1390 cm$^{-1}$), as well as the signature urethane carbonyl group at 1725 cm$^{-1}$, are clearly discernible.

The major difference between the TDI- and the MDI-derived polyurethanes is that the TDI-derived coatings were fully transparent, whereas the MDI-derived coatings appear "cloudy," which may limit their application potential.

# Chapter 3: Synthesis and Characterization of Polyepoxy/Amine Resins Derived from D.E.R. 332 (Olin Corporation) and Diethylenetriamine

## 3.1 A Polyepoxy/Amine Resins

D.E.R.™ 332 and diethylenetriamine were selected as a model system for polyepoxy/amine resins after consulting with Olin Corporation (a subsidiary of The Dow Chemical Company; Olin Corporation, 2019b). Whereas 2,2-Bis[4-(glycidyloxy) phenyl]propane, 4,4′-Isopropylidenediphenol diglycidyl ether is the major component of D.E.R.™ 325 or D.E.R.™ 3401, these mixtures that are used for concrete protection contain additives that may cloud the mechanistic studies performed here. Diethylenetriamine was used for similar reasons. It is the major component (>90% by weight) of D.E.H.™ 20 (Olin Corporation, 2019a), which is used as a curing agent (hardener) for D.E.R. agents. Using pure diethylenetriamine permits a clearer mechanistic insight into the reactivity of interactions of the study's protective coatings for concrete. The principal chemical reaction leading to a polyepoxy/amine resin is shown in Figure 3.1. Please note that under these conditions, a minor amount of 2-Bis[4-(glycidyloxy) phenyl]propane, 4,4′-Isopropylidenediphenol diglycidyl ether also undergoes homopolymerization, as this is typical for epoxy reagents (Ratna, 2003).
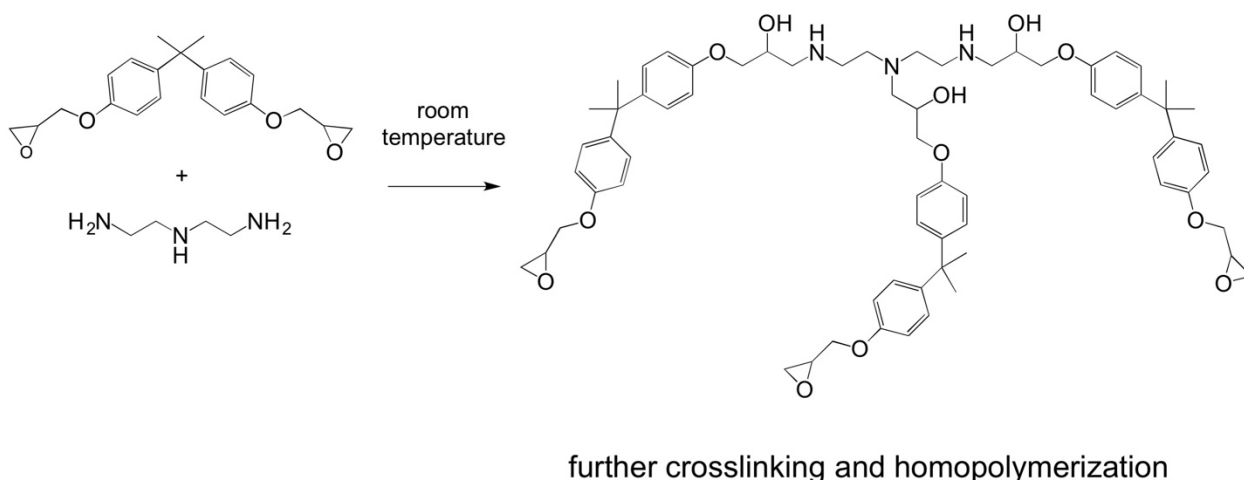


**Figure 3.1: Principal reactions during the thermal crosslinking of 2,2-Bis[4-(glycidyloxy) phenyl] propane, 4,4′-Isopropylidenediphenol diglycidyl ether with diethylenetriamine**
Source: Hara (1990)

The research team performed a series of six initial polymerization reactions with varying ratios of Bis[4-(glycidyloxy) phenyl]propane, 4,4′-Isopropylidenediphenol diglycidyl ether to diethylene-triamine (95:5, 90:10, 85:15, 82:18, 80:20, 78:22, all ratios are molar ratios) at 25 °C. The initial viscosity of the mixtures ranged from 4800 to 5200 mPa·s, which was in agreement with data provided by Olin Corporation (2019b). In Table 3.1, the initial viscosity, the viscosity after 60 minutes and the threshold of thermal stability, as determined by means of differential thermogravimetry analysis (DTA), are summarized.

**Table 3.1: Investigated Mixtures of D.E.R. ™ 332 and Diethylenetriamine**

| Test Mixture Number | Molar Ratio of D.E.R. ™ 332 to Diethylenetriamine | Initial Viscosity (mPa·s) | Viscosity after 60 min. (mPa·s) | Threshold of Thermal Decomposition |
|---|---|---|---|---|
| 0 | 100:0 | 4,200 | 4,200 | 360 °C[*] |
| 1 | 95:5 | 4,800 | 8,100 | 360 °C[*] |
| 2 | 90:10 | 4,850 | 12,200 | 365 °C |
| 3 | 85:15 | 5,100 | 23,500 | 365 °C |
| 4 | 82:18 | 5,150 | > 60,000[**] | 370 °C |
| 5 | 80:20 | 5,200 | > 60,000[**] | 370 °C |
| 6 | 78:22 | 5,200 | > 60,000[**] | 370 °C |

[*] Thermal polymerization was observed prior to heat-induced decomposition
[**] Maximum of measurable viscosity

Test mixture #4 (Molar Ratio of D.E.R. ™ 332 to Diethylenetriamine of 82:18) was selected for further characterization, because it formed fully transparent solid and/or coatings after 60 minutes of reacting at 25°C, whereas text mixtures #5 and #6 formed cloudy solids and/or coatings.

In Figure 3.2, the FTIR spectrum of test mixture #4 (Molar Ratio of D.E.R. ™ 332 to Diethylenetriamine of 82:18) is shown. The amine (NH) peak at 3100 cm$^{-1}$, as well as the aromatic CH transitions (> 3000 cm$^{-1}$, 1605 cm$^{-1}$, and 1505 cm$^{-1}$) and aliphatic CH transitions (<3000 cm$^{-1}$, 1450 cm$^{-1}$, and 1390 cm$^{-1}$) are clearly discernible.
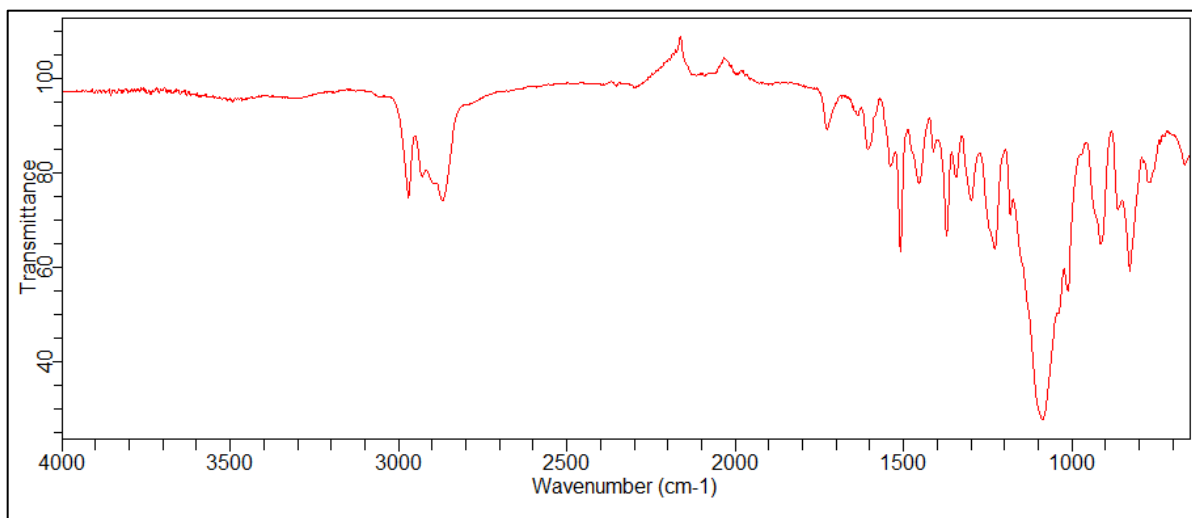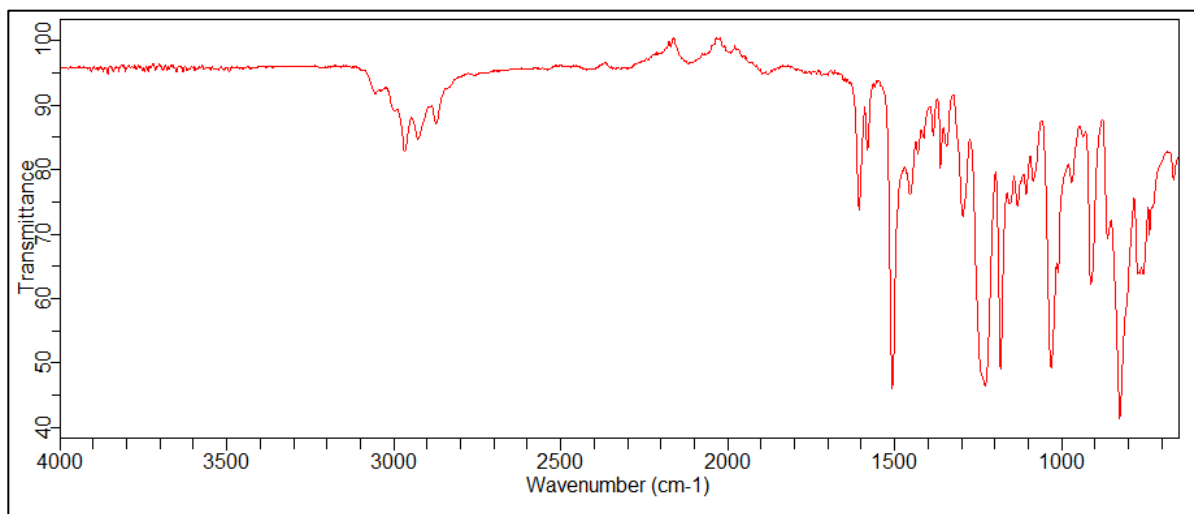
**Figure 3.2: FTIR of test mixture #4 on alumina after 60 minutes of curing reaction**
The transmission infrared spectrum (peaks go "down") shows peaks at 3100 cm$^{-1}$, > 3000 cm$^{-1}$, 1605 cm$^{-1}$, 1505 cm$^{-1}$, 1450 cm$^{-1}$, and 1390 cm$^{-1}$.

## 3.2 Summary of Phase I

In Phase 1 of this Kansas Department of Transportation (KDOT) funded research endeavor, the Bossmann group at Kansas State University has performed the synthesis and characterization of polyurethane resins from VORANOL 220-110 (DOW) and mixtures of TDI (toluene, diisocyanates) and MDI (methylene diphenyl diisocyanate), as well as polyepoxy/amine resins derived from (D.E.R. 332; Olin Corporation, 2019b) and diethylenetriamine.

After the successful synthesis and optimization of the required polymers, the project will now progress to Phase 2, in which potential interactions between both polymer types will be investigated. This study will focus on two principal modes of interactions: (a) physical mixtures of both types of polymers and (b) chemical experiments, in which the precursors for the formation of polyurethane coatings and polyepoxy/amine resins will be mixed and then allowed to react with each other. The research team anticipates observing cross-reactivity and will study its influence on polymer stability and general properties.

# Chapter 4: Synthesis and Characterization of Composite Polyisocyanate / Polyepoxyamine Resins from Previously Optimized VORANOL 220-110 (DOW) / TDI (Toluene, Diisocyanate) and MDI (Methylene Diphenyl Diisocyanate) Mixtures and D.E.R. 332 (Olin Corporation) / Diethylene-Triamine Mixtures

**Phase 2:** Investigation of potential interactions between **polyepoxy composite resins** and **polyisocyanate composite resins.** This study will focus on chemical experiments, in which the precursors for the formation of polyurethane coatings and polyepoxy/amine resins have been mixed and then allowed to react with each other. Physical mixtures of the polymers were investigated as well. However, de-mixing occurred over a wide range of concentrations.

## 4.1 Synthesis and Thermal Decomposition Study of co-Polyisocyanate/Poly-epoxyamine Resins

VORANOL 220-110 is a polyether polyol homopolymer (molecular weight ~1000 g/mole), derived from propylene oxide. It contains two terminal hydroxyl groups, which react with the isocyanate groups of ortho-, para-toluene diisocyanate (93%, shown) and ortho-, ortho- toluene diisocyanate (6%, not shown) to linear polyurethane chains and then polyurethane networks (with ortho-, ortho-, para-toluene triisocyanate (TTI), 1%, not shown). 2,2-Bis[4-(glycidyloxy) phenyl]propane, 4,4′-Isopropylidenediphenol diglycidyl ether is the major component of D.E.R.$^{TM}$ 325 or D.E.R.$^{TM}$ 3401. Diethylenetriamine is used as a reactive amine component. Based on previous experiments, the mixing ratios that were determined to create to the best polyisocyanate and polyepoxyamine coatings are listed in Table 4.1.

**Table 4.1: Mixing Ratios for Optimized co-Polyisocyanates/Polyepoxyamine Resins**

| Molar Ratio of VORANOL 220-100 to TDI | Initial Viscosity (mPa·s) | Viscosity after 60 min. (mPa·s) | Threshold of Thermal Decomposition |
|---|---|---|---|
| 48:52 | 280 | > 60,000[*] | 345 ℃ |
| Molar Ratio of VORANOL 220-100 to MDI | Initial Viscosity (mPa·s) | Viscosity after 60 min. (mPa·s) | Threshold of Thermal Decomposition |
| 48:52 | 380 | > 60,000[*] | 365 ℃ |
| Molar Ratio of D.E.R. $^{TM}$ 332 to Diethylenetriamine | Initial Viscosity (mPa·s) | Viscosity after 60 min. (mPa·s) | Threshold of Thermal Decomposition |
| 80:20 | 5,200 | > 60,000[*] | 370 ℃ |

[*]Maximum of measurable viscosity

The principal reaction between VORANOL 220-110 and TDI is shown in Figure 4.1.
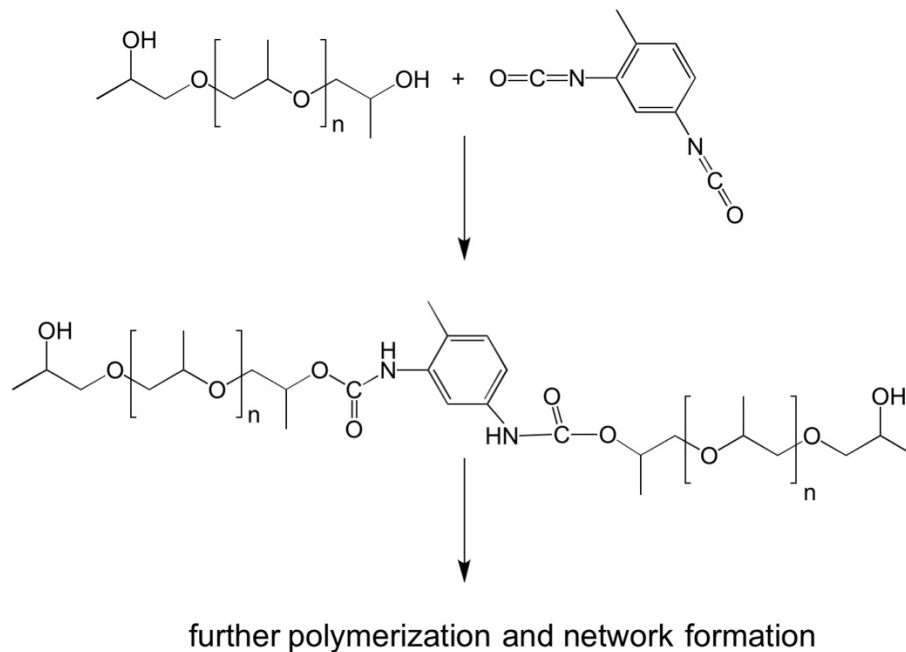


**Figure 4.1: Principal reactions during the thermal crosslinking of VORANOL 220-110 and TDI**
Source: Akindoyo et al (2016)

The principal reaction of 2-Bis[4-(glycidyloxy) phenyl]propane, 4,4′-Isopropylidenediphenol diglycidyl ether with diethylenetriamine is shown in Figure 4.2.
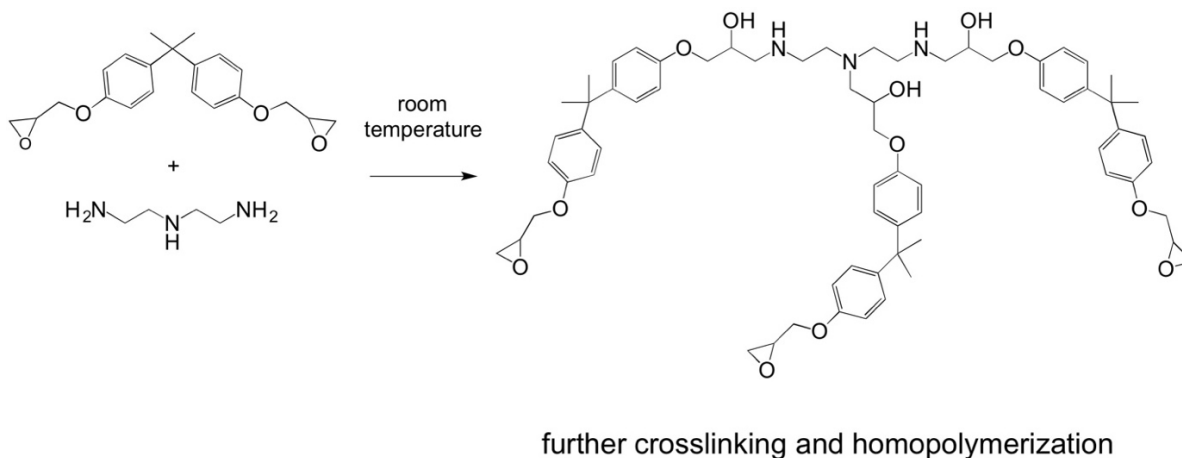


**Figure 4.2: Principal reactions during the thermal crosslinking of 2,2-Bis[4-(glycidyloxy) phenyl] propane, 4,4′-Isopropylidenediphenol diglycidyl ether with diethylenetriamine**
Source: Hara (1990)

Seven co-polymerization reactions were performed with varying ratios of **VORANOL 220-110/TDI/MDI (48/26/26, Resin A)** and **D.E.R. ™ 332 to Diethylenetriamine (80:20, Resin B)** (95:5, 90:10, 75:25, 50:50, 25:75, 10:90, 5:95, all ratios are weight ratios) at 25 ℃. The initial viscosity of the mixtures ranged from 320 to 5,000 mPa·s, which agreed with data provided by Olin Corporation (2019b), and the optimization experiments in Phase 1. In Table 4.2, the initial viscosity, the viscosity after 60 minutes and the threshold of thermal stability, as determined by means of differential thermogravimetry analysis (DTA), are summarized. As summarized in Table 4.2, the process of copolymerization leads to higher thermal decomposition temperatures of co-resins, compared to either polyisocyanate or polyepoxyamine resin. The best mixing ratio was 75% polyisocyanate to 25% polyepoxyamine resin. However, as shown in Table 4.2, all mixtures between 90% polyisocyanate to 10% polyepoxyamine and 5% polyisocyanate to 95% polyepoxyamine performed better than both mono-resins.

**Table 4.2: Initial and Final Viscosities of Optimized co-Polyisocyanate (A)/Polyepoxyamine (B) Resins, as well as their Thresholds of Thermal Decomposition (as measured by Differential Thermogravimetry Analysis)**

|  | Weight Ratios of Resin (A), Resin (B) | Initial Viscosity (mPa·s) | Viscosity after 60 min. (mPa·s) | Threshold of Thermal Decomposition |
|---|---|---|---|---|
| 1 | 100:0 | 360 | > 60,000[*] | 345 ℃ |
| 2 | 95:5 | 610 | > 60,000[*] | 365 ℃ |
| 3 | 90:10 | 920 | > 60,000[*] | 390 ℃ |
| 4 | 75:25 | 1,680 | > 60,000[*] | 395 ℃ |
| 5 | 50:50 | 2,620 | > 60,000[*] | 390 ℃ |
| 6 | 25:75 | 3,540 | > 60,000[*] | 385 ℃ |
| 7 | 10:90 | 4,130 | > 60,000[*] | 385 ℃ |
| 8 | 5:95 | 4,570 | > 60,000[*] | 380 ℃ |
| 9 | 0:100 | 5,200 | > 60,000[*] | 370 ℃ |

[*] Maximum of measurable viscosity

Based on the research team's principal knowledge of the chemistry occurring during resin formation (Figure 4.1 and Figure 4.2) and the findings summarized in Table 4.2, NMR experiments to determine potential crosslinking reactions between the polyisocyanate and the polyepoxyamine chemistries were performed.

As a control experiment, the physical mixtures of Resin (A) and Resin (B) were also investigated in the same weight ratios as described in Table 4.2. No enhancement of the threshold

of thermal decomposition was found, as indicated in Figure 4.3. These results conclude that de-mixing occurs when mixtures of polyisocyanate and the polyepoxyamine resins are heating and that their decomposition is determined by the least heat stable resin.
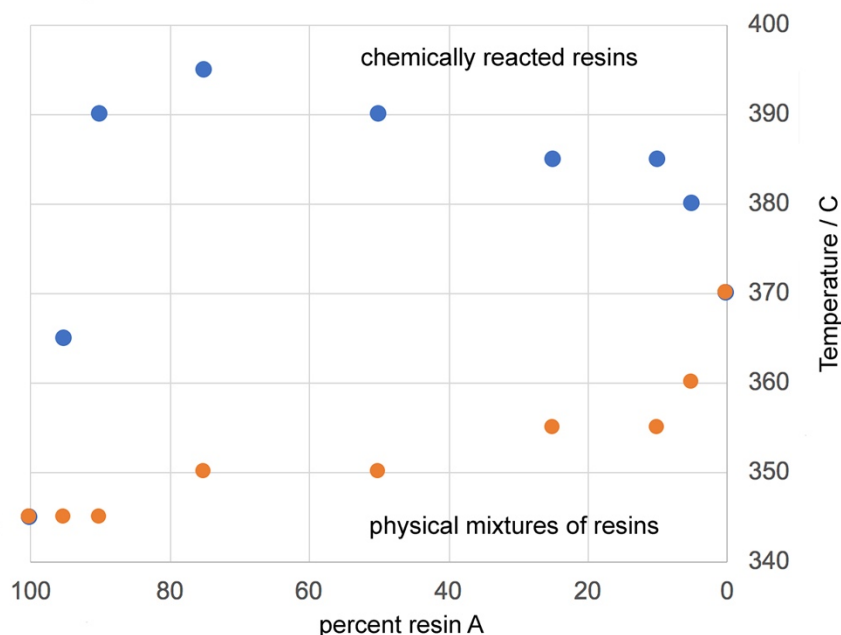


**Figure 4.3: Thresholds of Thermal Decomposition for Chemically Reacted Resins (Table 4.2, blue symbols) and Physical Mixtures of Resins (A) and (B) as Control Experiments (orange symbols)**

The blue dots start at 345 ℃ (100% A) and rise to 365 ℃ (95% A / 5% B), 390 ℃ (90% A / 10% B), and 395 ℃ (75% A/ 25% B). They then decline to 385 ℃ (50% A / 50% B), 385 ℃ (25% A / 75% B and 10% A / 90% B) to reach 370 ℃ at 100% B. The orange dots start at 345 ℃ (100% A, 95% A / 5% B, and 90% A / 10% B) and increase to 350 ℃ (75% A/ 25% B and 50% A / 50% B), 355 ℃ (25% A / 75% B and 10% A / 90% B), 360 ℃ (5% A / 95% B) and finally 370 ℃ (100% B).

## 4.2 NMR Studies of Cross-Reactions Occurring between Polyisocyanates and Polyepoxyamines

After establishing an enhanced threshold of thermal decomposition in Polyisocyanate and Polyepoxyamine co-resins, the chemical reasons for this behavior were investigated by means of $^1$H-NMR spectroscopy.

A series of five co-polymerization reactions were performed with varying ratios of **VORANOL 220-110/TDI/MDI (48/26/26, Resin A)** and **D.E.R. $^{TM}$ 332 to Diethylene-triamine (80:20, Resin B)** (90:10, 75:25, 50:50, 25:75, 10:90, all ratios are weight ratios) at 25 ℃. 100 μl of these reactive mixtures was dissolved in 1.0 mL of deuterated dimethyl sulfoxide (D$_6$MSO) as

non-reactive NMR solvent. The reaction mixtures were allowed to react at exactly 25 °C for 60 minutes and were then measured. The results are shown in Figure 4.4 and Figure 4.5 in comparison with the mono-resins (A) and (B).
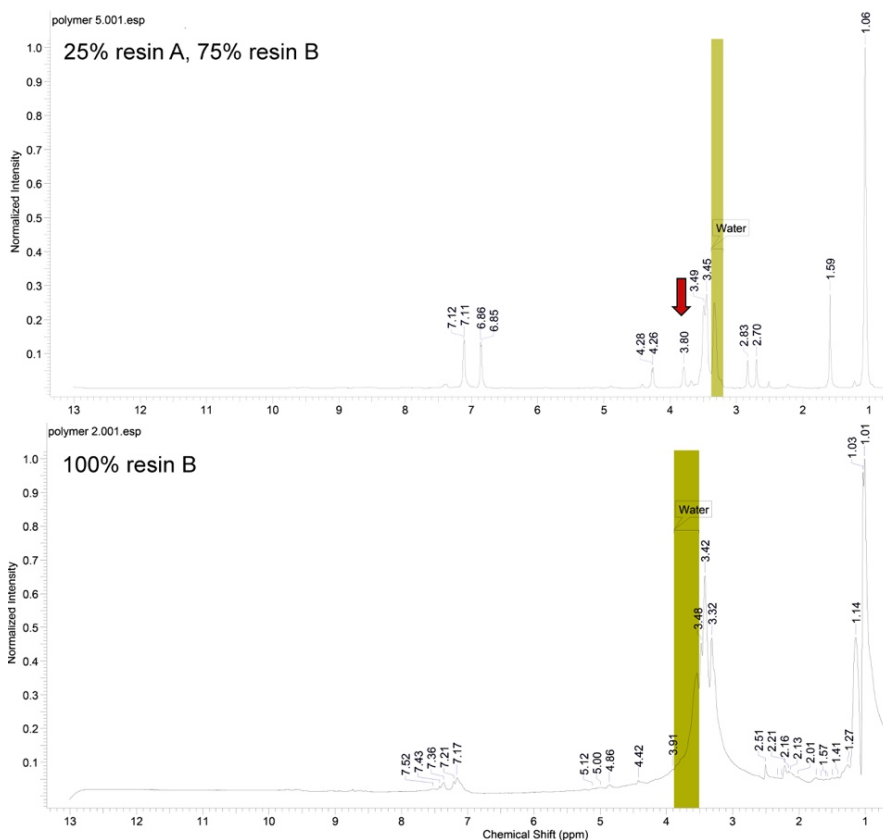


**Figure 4.4: $^1$H-NMR spectrum of 25% Resin (A), 75% Resin (B) and 100% Resin (B) in D$_6$MSO (Bruker Avance III, 600 MHz)**

The novel set of $^1$H-NMR peaks that are not present in either Resin (A) or (B) is marked with a red arrow. Upper Figure (25% Resin A, 75% Resin B): $^1$H NMR peaks are discernible at δ = 7.52, 7.11, 6.86, 6.85, 4.28, 4.26, 3.80 (new peak), 3.49, 3.45, 2.83, 2.70, 1.59, and 1.06 ppm. All peaks are absorptive (they show upwards). Lower Figure (100% Resin B): $^1$H NMR peaks are discernible at δ = 7.12, 7.43, 7.36, 7.21, 7.17, 5.12, 5.00, 4.86, 4.43, 3.91, 3.48, 3.32, 2.51, 2.21, 2.16, 2.13, 2.01, 1.57, 1.41, 1.27, 1.14, 1.03, and 1.01 ppm. All peaks are absorptive (they show upwards).
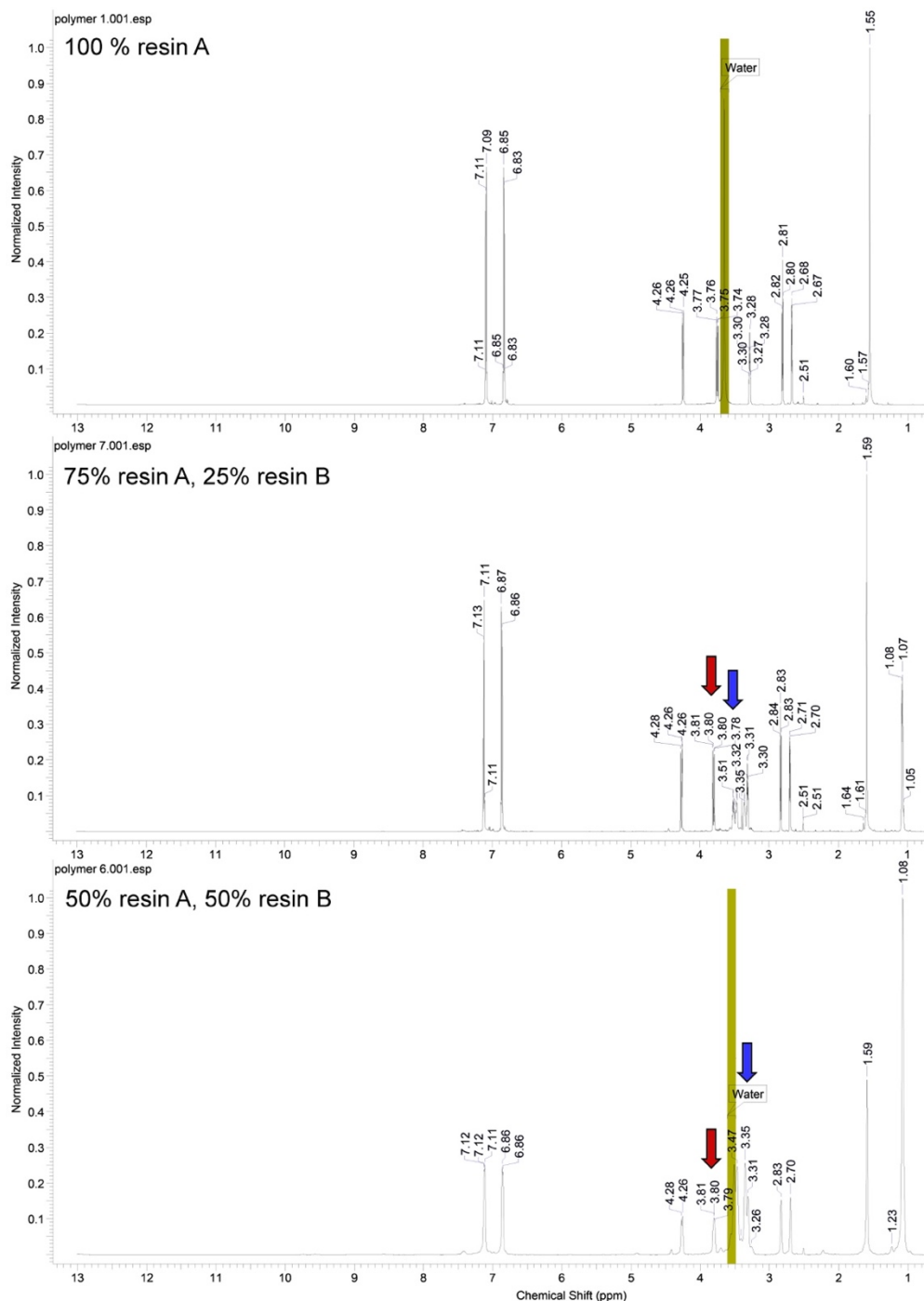
**Figure 4.5:** ¹H-NMR spectrum of 100% Resin (A), 75% Resin (A), 25% Resin (B) and 50% Resin (A), 50% resin in D6MSO (Bruker Avance III, 600 MHz)

The novel sets of ¹H-NMR peaks that are not present in either Resin (A) or (B) are marked with a blue and a red arrow. Upper Figure (100% Resin A): ¹H NMR peaks are discernible at δ = 7.12, 7.11, 7.09, 6.85, 6.83, 6.84, 4.27, 4.26, 4.25, 3.77, 3.76, 3.75, 3.74, 3.31, 3.30, 3.29, 3.28, 3.27, 2.82, 2.81, 2.80, 2.68, 2.67, 2.51, 1.60, 1.57, and 1.55 ppm. All peaks are absorptive (they show upwards). Middle Figure (75% Resin B / 25% Resin A): ¹H NMR peaks are discernible at δ = 7.13, 7.12, 7.11, 6.87, 6.86, 4.28, 4.27, 4.26, 3.80, 3.79, 3.78 (new peaks, marked in red), 3.51, 3.32, 3.31 (new peaks, marked in blue), 2.84, 2.83, 2.71, 2.70, 2.51, 1.64, 1.61, 1.59, 1.08, 1.07, and 1.05 ppm. All peaks are absorptive (they show upwards). Lower Figure (50% Resin A / 50% Resin B): ¹H NMR peaks are discernible at δ = 7.12, 7.11, 6.86, 6.85, 4.28, 4.26, 3.81, 3.80, 3.79 (new peaks, marked in red), 3.35, 3.31 (new peaks marked in blue), 3.26, 2.83, 2.70, 1.59, 1.23, and 1.08.

17

Based on the chemical shifts of the additional ${}^1$H-NMR peaks that were observed in polyisocyanate/polyepoxyamine co-resins, two types of cross-reactions have been identified that do not occur in the respective mono-resins.
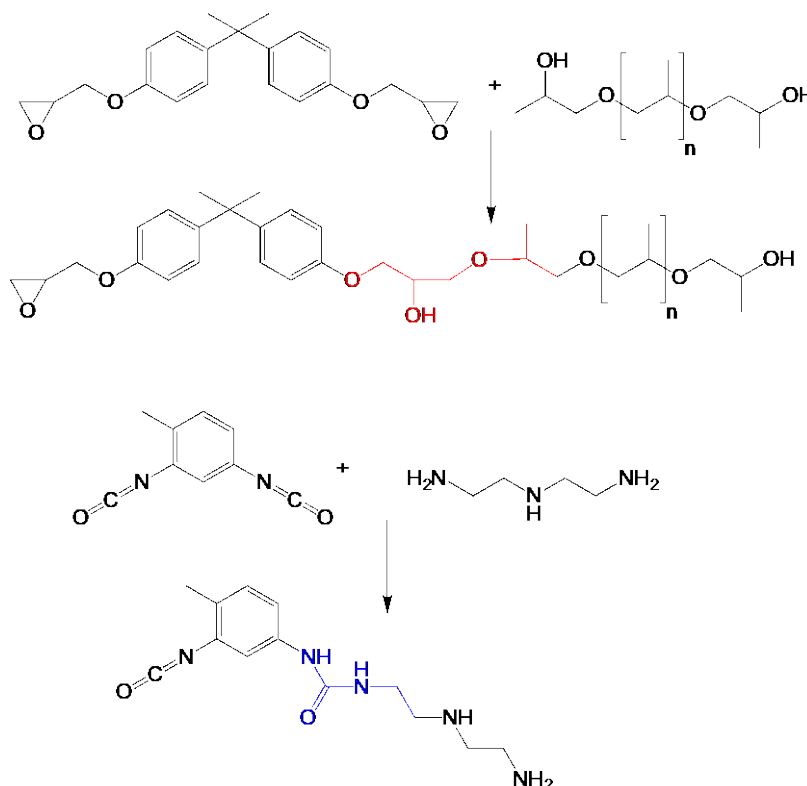


**Figure 4.6: Cross-reactions occurring in polyisocyanate/polyepoxyamine co-resins, as observed by ${}^1$H-NMR spectroscopy**

The cluster of novel peaks around $\delta = 3.8$ ppm results from the reaction of an epoxy-group of 2,2-Bis[4-(glycidyloxy) phenyl] propane, 4,4′-Isopropylidenediphenol diglycidyl ether with the terminal hydroxyl group of Voranol 220. The cluster of novel peaks around $\delta = 3.5$ ppm results from the reaction of a primary amine group of diethylenetriamine with toluene diisocyanate. The resulting urea groups are mainly responsible for the observed increase in decomposition temperature of the co-resins.

## 4.3 Summary of Phase 2

In Phase 2 of this Kansas Department of Transportation (KDOT) funded research endeavor, the Bossmann group at Kansas State University has performed the synthesis and characterization of polyisocyanate/polyepoxyamine co-resins from previously optimized polyisocyanate and polyepoxyamine resins. Improved thresholds of thermal decomposition were observed by means of differential thermogravimetry (DTA) for all synthesized co-resins. The maximum of thermal

stability occurred at 395 °C and was observed at a mixing ratio of 75% polyisocyanate and 25% polyepoxyamine resin precursors and 60 minutes of reaction at 25 °C.

In order to discern the chemical reasons for the observed synergy, the research team has conducted ^{1}H-NMR experiments, in which two types of cross-reactions have been identified between polyisocyanate and polyepoxyamine resin precursors: the formation of an ether-bond by means of an epoxide ring-opening reaction, and the formation of a urea-type bond between a primary amine and an isocyanate. These urea-type bonds are most likely responsible for the observed increase in thermal stability.

# Chapter 5: Specific Images using Different Image Methods of Concrete Model Wafers

**Phase 3:** Investigation of potential interactions of **polyepoxy/polyisocyanate composite co-resins** with the surfaces of concrete model wafers provided by KDOT in comparison with a **polyepoxy resin and** a **polyisocyanate composite resin.** This chapter reports the outcomes of the **Atomic force microscopy (AFM)** experiments on surfaces and the **Magnetic resonance imaging (MRI)** experiments with uncoated and coated concrete model wafers.

## 5.1 Atomic Force Microscopy Investigations of Untreated and (Composite) Polymer Treated Concrete Model Wafers (Provided by KDOT)

Atomic force microscopy images were taken by a Nanoscope AFM image system (Digital Instruments) utilizing TESPA-HAR probes in tapping mode. The spring constant of the tip was 50 Newton/meters (N/m) and the frequency was 350 kHz. The set point, P gain, and I gain were set at 1.2, 0.6, and 0.5, respectively. The images were gathered with 256×256-pixel resolution at a scan rate of 1 Hz. The images were then analyzed by the Nanoscope software (Bruker).
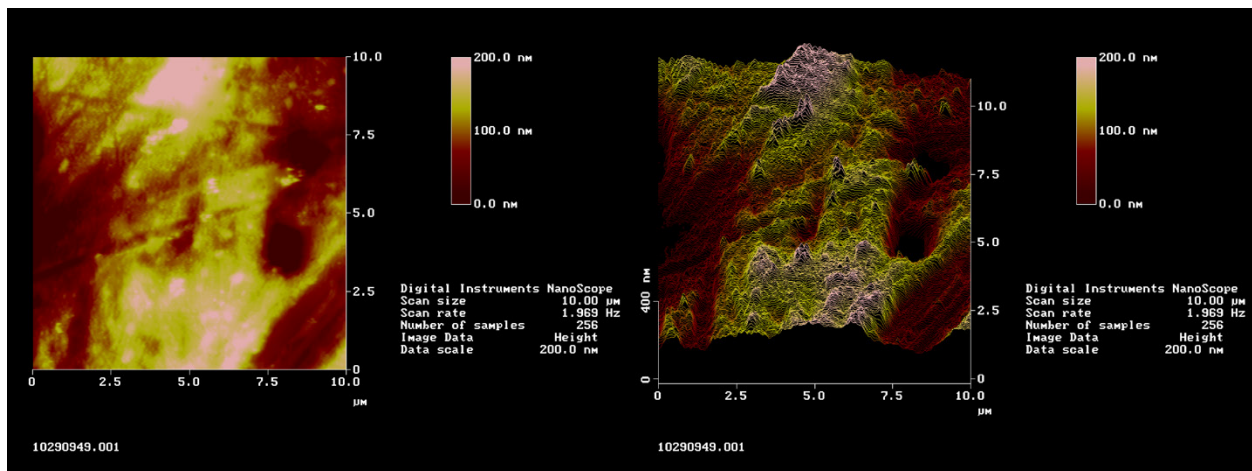


**Figure 5.1: AFM images (tapping mode, left) and height profiles (right) of a typical concrete wafer (Type 1 provided by KDOT, smoother apparent surface)**

The image on the left shows an irregular pink and yellow structure on brown background. The pink and yellow zones correspond to elevated regions, whereas the brown regions are lower. The height difference between high and low consists of 200 nanometers (nm). The image on the right shows the corresponding line drawing image. The elevated regions form a "nano-mountain range" in the middle of the image (10 × 10 micrometers).

From the AFM images summarized in Figure 5.1, it is discernible that typical height variations at the surface of apparently smooth concrete wafers (Type 1) are in between 0 and 200 nm. This can be considered very smooth according to technical standards. In order to use a more realistic model-system for concrete surfaces, KDOT fabricated Type 2 concrete wafers from cement paste. It has been determined that the surface of Type 2 concrete wafers was significantly rougher (Figure 5.2); height variations were in between 0 and 2000 nm, which is 10 times rougher than Type 1 wafers. However, this result should not be overinterpreted (see MRI experiments described below), because AFM is sampling only very small surface areas (10 micrometers × 10 micrometers).
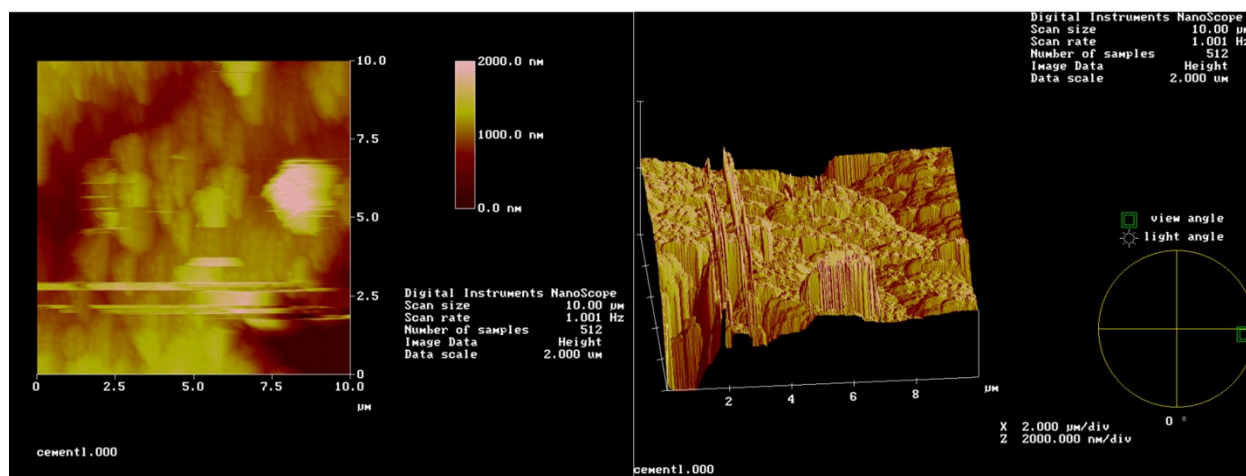


**Figure 5.2: AFM images (tapping mode, left) and height profiles (right) of a typical concrete wafer (Type 2 provided by KDOT, made from cement paste)**
The image on the left shows irregular pink and yellow structures on brown background. The pink and yellow structures correspond to elevated regions, whereas the brown regions are lower. The height difference between high and low consists of 2,000 nm. The image on the right shows the corresponding line drawing image. The elevated regions form a "nano-mountain landscape" in the middle of the image (10 x 10 micrometers).

Before performing AFM measurements of resins and co-resins on concrete wafer surfaces, a series of preliminary tests were run, in which the (co-resin) precursors were allowed to react on the wafer surfaces for 60 minutes at 25 °C. The compositions of the reactive mixtures were appropriated from Table 3.1.
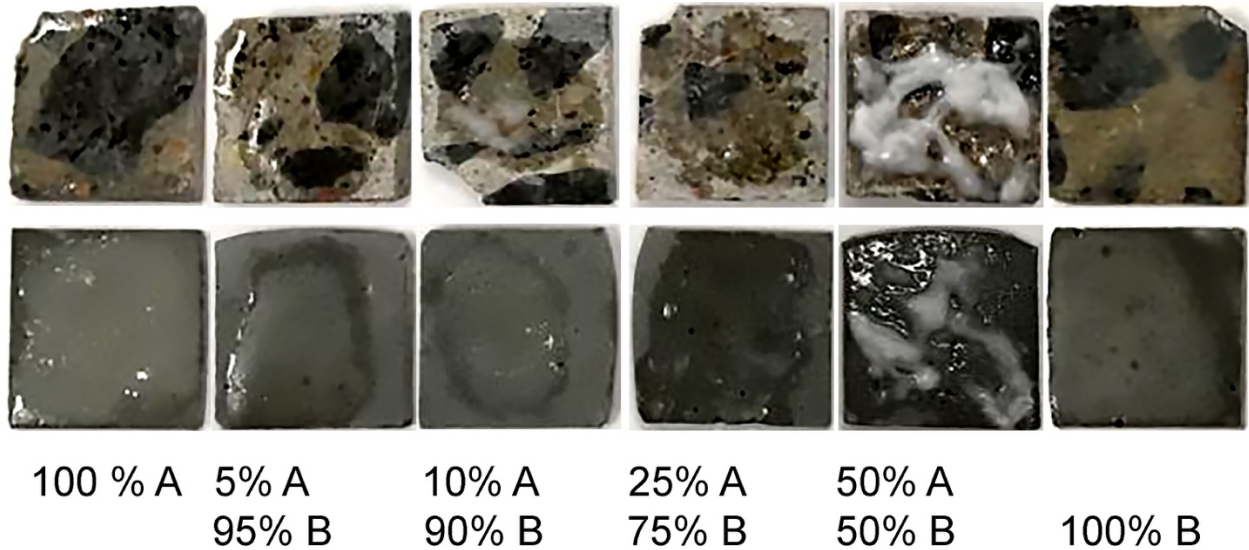
**Figure 5.3: Optical AFM images of Resins (A: polyisocyanate, B: polyepoxyamine resins) and co-resins synthesized at the surface of the wafers from resin precursors**

Upper row: Type 1 concrete wafers were employed. Lower row: Type 2 concrete wafers made from cement paste were used. Type 1 wafers look speckled (dark: basalt regions, white: mainly quartz and mica regions). Type 2 wafers look uniformly gray. 100% A resin, as well as 5% A / 95% B, 10% A / 90% B, and 25% A / 75% B resins form colorless coatings on Type 1 wafers, and opaque coatings on Type 2 wafers. At 50% A / 50% B resins, de-mixing occurs, leading to incomplete coating of both types of wafer with a whitish material. 100% B resin adheres to both types of wafer and forms an almost transparent coating.

As it can be discerned from Figure 5.3, the cross-reactivity between the two types of resins, polyisocyanate and polyepoxyamine, has a detrimental effect on the surface smoothness of both types of concrete wafers. The formation of urea-type bonds prevents the formation of smooth surfaces, which are absolutely mandatory for any meaningful application of the co-resins in the area of transportation. Although the thermal stability of these co-resins is significantly enhanced, the decision was made to abandon the use of any co-resins and instead focus the research on the comparison of polyisocyanate and polyepoxyamine resins on concrete wafers. Both resins were synthesized by spreading 1.0 mL of reactive resin precursors onto the surface of the 1 cm × 1 cm wafers. The mixtures were allowed to react for 60 minutes at 25 °C.

The AFM images below (Figure 5.4 and Figure 5.5) are of polyisocyanate or polyepoxyamine resin layers on Type 2 wafers. It is clearly discernible that both types of resins react differently on the wafer surface.
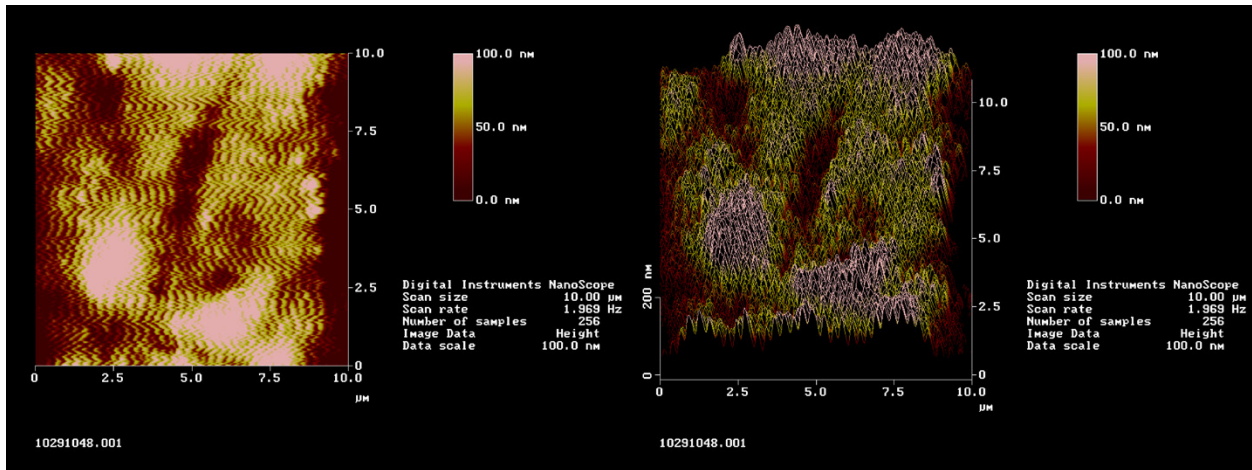
**Figure 5.4: AFM images (tapping mode, left) and height profiles (right) of a polyisocyanate resin (A) on a Type 2 wafer provided by KDOT (made from cement paste)**

The image on the left shows irregular pink and yellow structures on brown background. The pink and yellow structures correspond to elevated regions, whereas the brown regions are lower. The height difference between high and low consists of 100 nm. The image on the right shows the corresponding line drawing image. The elevated regions form a "flat landscape with a couple of pockets" (10 x 10 micrometers). It is noteworthy that the polyisocyanate resin (A)-coated wafer was much smoother than the uncoated Type 2 wafer (factor 20).

As shown in Figure 5.4, the polyisocyanate resin (A) that was directly synthesized on the surface of Type 2 wafers decreased the surface roughness by a factor of 20. The resulting surface is apparently smooth (although looking at Figure 5.4 can be deceiving). The reason for the observed substantial decrease in surface roughness is that resin (A) was able to fill the "valleys" on the surface of the concrete wafer.
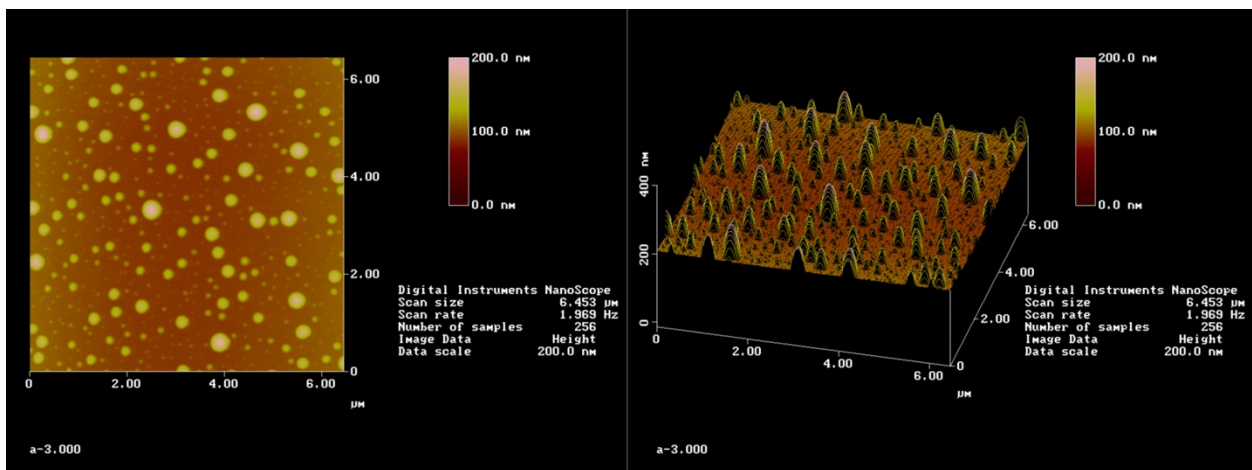


**Figure 5.5: AFM images (tapping mode, left) and height profiles (right) of a polyepoxyamine resin (B) on a Type 2 wafer provided by KDOT (made from cement paste)**

The pink and yellow structures correspond to elevated regions, whereas the brown regions are lower. The height difference between high and low consists of 200 nm. The image on the right shows the corresponding line drawing image. The elevated regions form a "flat landscape with step conical mountains" (10 × 10 micrometers). It is noteworthy that also the polyepoxyamine resin (B)-coated wafer was much smoother than the uncoated Type 2 wafer (factor 20).

Figure 5.5 indicates that polyepoxyamine resin (B) that was directly synthesized on the surface of Type 2 wafers was able to form "super-flat" surfaces, on which "resin-pillars" of 30 to 110 nm in height were observed. Resin (B) was able to fill in all the "valleys" (= lower v-section). The observed "pillars" are also observed in numerous superhydrophobic surfaces (Lotus effect; Yamamoto et al., 2015) and often the cause for hydrophobic or even super-hydrophobic behavior. Considering the function of Resin (B) (sealing of concrete structures in transportation), this is certainly a significant advantage compared to Resin (A). Polyepoxy-based resins appear to be clearly superior in coating concrete model wafers, compared to polyisocyanate resins.

## 5.2 Magnetic Resonance Imaging Investigations of Untreated and (Composite) Polymer Treated Concrete Model Wafers (Provided by KDOT)

All MRI Pulse Sequences that have been utilized for studying the resin-covered concrete wafers were developed by Bruker Biospin (Tang, Zhang, Chen, & Huang, 2015). The principal advantage of using a 14.1T $B_0$ field is that according to Boltzmann statistics, the difference between the populations of parallel and antiparallel spins increases with magnetic field strength ($B_0$), leading to signal-to-noise enhancement and the requirement of shorter acquisition times for image-guided therapy (Heidemann et al., 2006). The greatest challenge of using high fields for MRI imaging is that T1 relaxation times (longitudinal magnetization recovery) increase with $B_0$, whereas T2 (transverse magnetization decay) decreases. The effects of modifications in relaxation times are such that sequences have to be adjusted to comply with slower longitudinal relaxation, shortened TE (echo time) due to reduced T2, to restore a significant T1 contrast (Inversion, MDEFT: modified driven equilibrium Fourier-transform). Typically, conventional pulse sequences are converted into spin echo sequences to compensate for shorter T2 relaxation times. More than the signal-to-noise ratio, it is the contrast-to-noise ratio that provides an objective comparison of the examinations performed with different field $B_0$. Resin (A) (polyisocyanate resin) and Resin (B) (polyepoxyamine resin) were synthesized on the surfaces of Type 2 wafers, as described above.

However, before the structure of the resins on wafers could be discerned, the wafers (Types 1 and 2) were studied by means of MRI. Since the wafers are important models for the interaction of resins with concrete surfaces, they themselves have to be thoroughly analyzed.
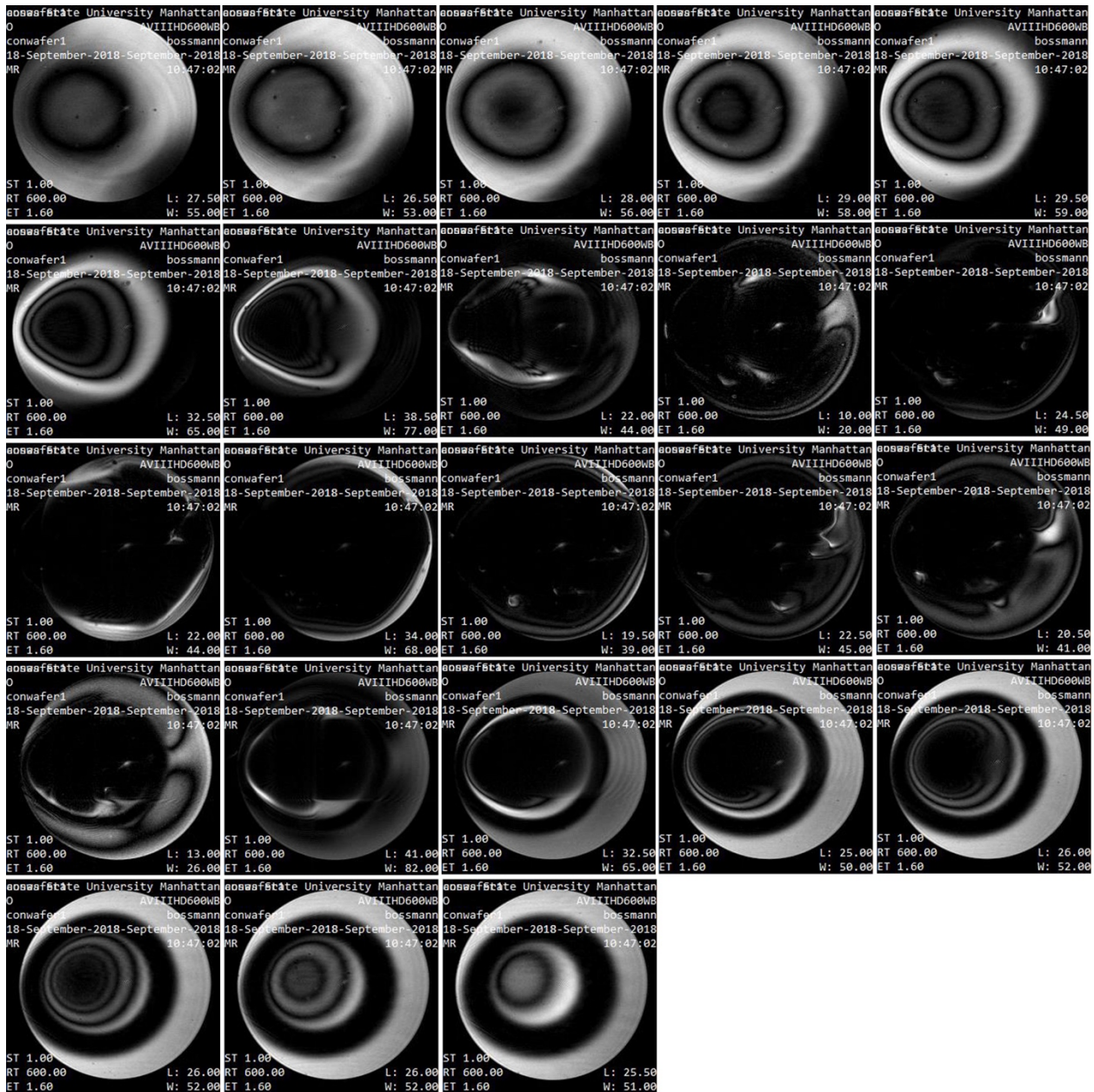
**Figure 5.6: Magnetic Resonance Imaging (MRI) of a Type 1 concrete wafer (embedded in a polyacrylate gel)**

The MRI contrast is visualizing mobile water within the wafer's structure. The "slices" proceed from the upper left corner to the lower right corner. Each slice has a thickness of 0.175 mm. The regions at the exterior of the Type 1 wafer are bright, due to the presence of protons (water). The interior is dark, due to the absence of protons. The transition of bright to dark regions leads to the formation of concentric ring structures. In the middle of Type 1 wafers, imperfections (visible as "bubbles") can be discerned.

As it can be seen in Figure 5.6, the resolution in the interior of the wafer is compromised. This is due to the absence of mobile water and due to the presence of paramagnetic cations (most likely iron).
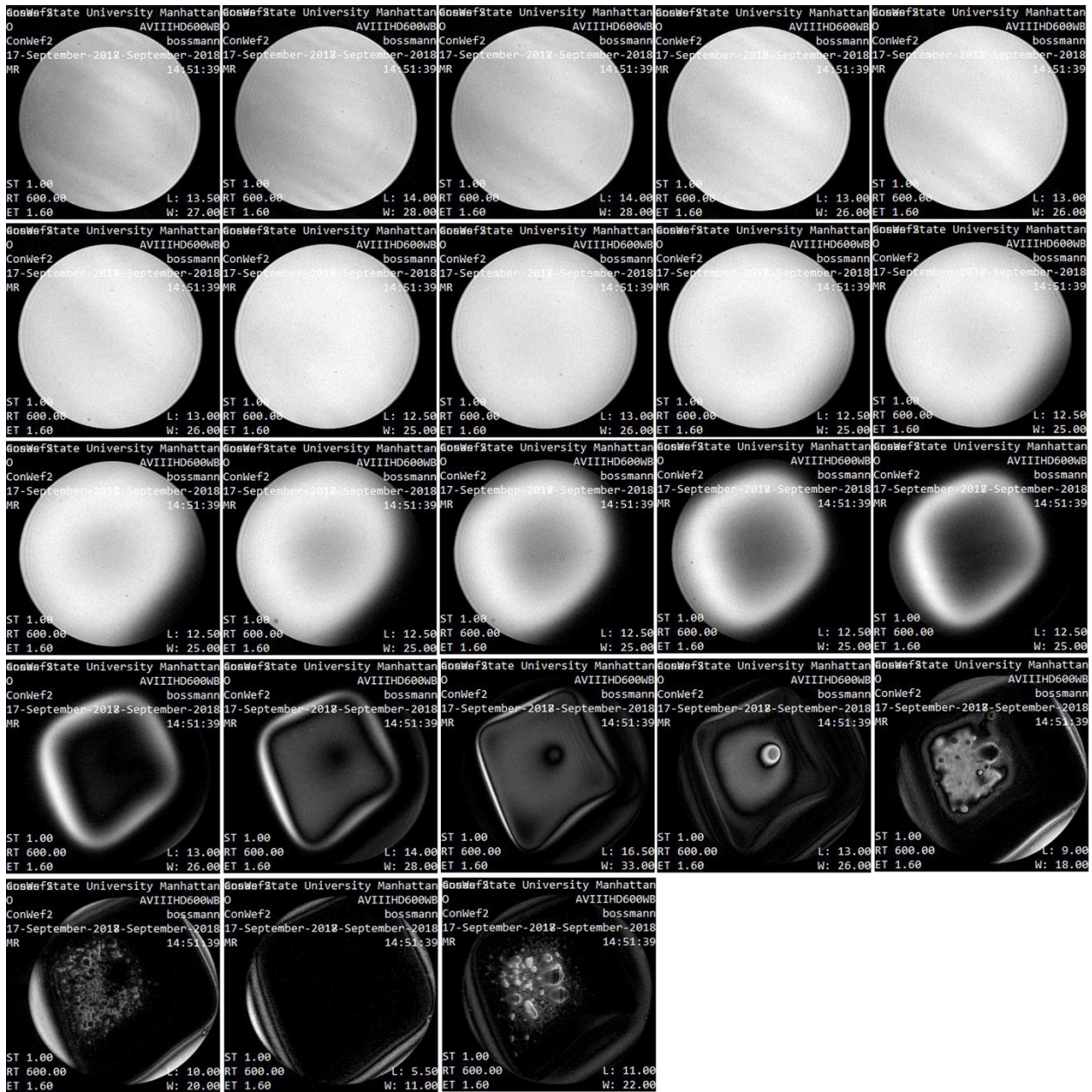
**Figure 5.7: Magnetic Resonance Imaging (MRI) of a Type 2 concrete wafer (embedded in a polyacrylate gel)**

The MRI contrast is visualizing mobile water within the wafer's structure. The "slices" proceed from the upper left corner to the lower right corner. Each slice has a thickness of 0.175 mm. The regions at the exterior of the Type 2 wafer are bright, due to the presence of protons (water). The interior is dark, due to the absence of protons. The transition of bright to dark regions leads to the formation of concentric ring structures. In the middle of Type 2 wafers, imperfections (visible as grainy structures) can be discerned.

**Figure 5.8: Magnetic Resonance Imaging (MRI) of a polyisocyanate resin (A) on the surface of a Type 2 concrete wafer (embedded in a polyacrylate gel)**

The "slices" proceed from the upper left corner to the lower right corner. Each slice has a thickness of 0.175 mm. The regions at the exterior of the Type 2 wafer are bright, due to the presence of protons in the adhesive polymer coating. The interior is dark, due to the absence of protons. The transition of bright to dark regions leads to the formation of concentric ring structures. In the middle of Type 2 wafers, imperfections (visible as grainy structures) can be discerned. The region of polyisocyanate resin (A) coating is very uniform, as seen from the absence of discernible features.

It has been observed that Type 2 wafers feature discernibly smoother concrete surfaces than Type 1 wafers. As it can be seen in Figure 5.7, the resolution that can be achieved with Type 2 wafers is superior to that of the Type 1 wafers, mostly because their water content is higher and paramagnetic ions are virtually absent. However, in the interior, water-filled cavities (black) and

27

air bubbles (white internal surfaces) were observed. Therefore, it may be advantageous to study a third series of wafers by means of MRI, which have been prepared according to an improved procedure. The ideal wafer should contain neither air nor water bubbles.



**Figure 5.9: Magnetic Resonance Imaging (MRI) of a polyisocyanate resin (A) on the surface of a Type 2 concrete wafer (embedded in a polyacrylate gel)**

Enlarged Slices 9, 10, 11, and 12 of Figure 5.8 are shown. Each slice has a thickness of 0.175 mm. The "slices" proceed from the upper left corner to the lower right corner. Each slice has a thickness of 0.175 mm. The interior of the wafer, which is shown here, is dark, due to the absence of protons. In the middle of Type 2 wafers, imperfections (visible as grainy structures) can be discerned. They can be discerned as the surface of stones that are embedded by the concrete wafer.

As shown in Figure 5.8 and Figure 5.9, the polyisocyanate resin (A) forms a very smooth layer on Type 2 concrete wafers of 1.56 mm thickness. Only a couple of small imperfections can be seen at the surface (Slices 1 and 2 in Figure 5.8). However, starting from a depth of 1.57 nm, the presence of water and air bubbles can be discerned. Whereas air bubbles have the potential to decrease the interface between concrete and coating, water bubbles can be truly detrimental, because they prevent chemical adhesion and lead potentially to frost damage and detachment of the protective coating. At this point in the investigation of the resin-concrete interface, it is likely that these air and water bubbles were already present in the wafer (Figure 5.7) before the coating was applied. However, it would be preferable to repeat this experiment with a wafer free of air and water bubbles to make sure that none of these structures are formed during the chemical binding process of the resin to the concrete.

As shown in Figure 5.10 and Figure 5.11, the thickness of the polyepoxyamine coating (Resin B) of the Type 2 concrete wafer is 1.05 mm. In agreement with the AFM findings reported above, the polyepoxyamine coating is very homogeneous and practically free of imperfections. However, when a depth of 1.1 mm is reached, mostly air bubbles and a few (black) water bubbles can be discerned. In analogy to the results for the coating of a Type 2 concrete wafer with a polyisocyanate coating (Resin A), it is assumed that virtually all the air bubbles were present within the concrete material before the coating was performed. However, it is interesting that significantly fewer water bubbles were observed after the coating process with Resin (B) was completed. This may be due to the chemical reaction of the epoxide precursors with the concrete-bound water.
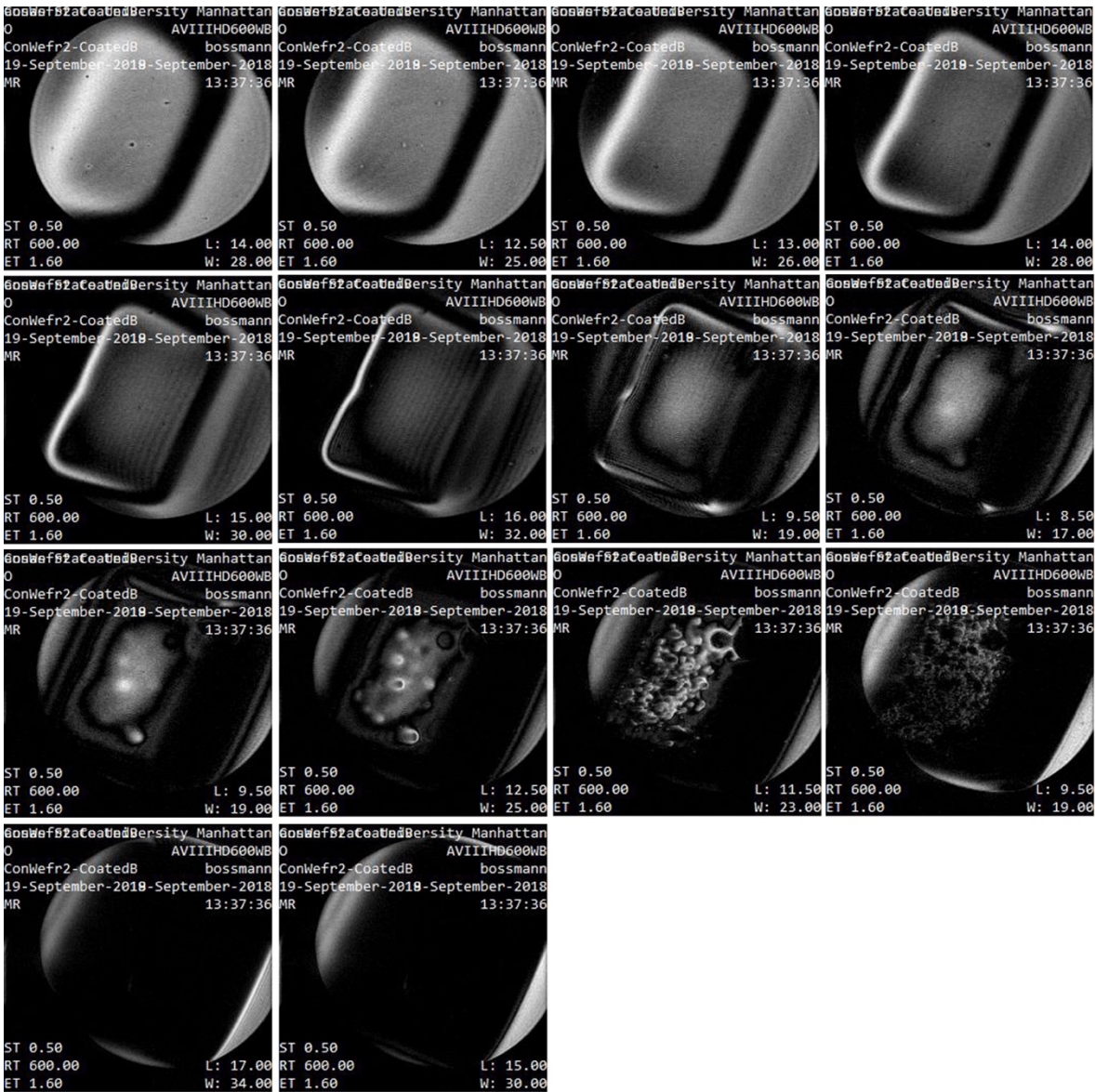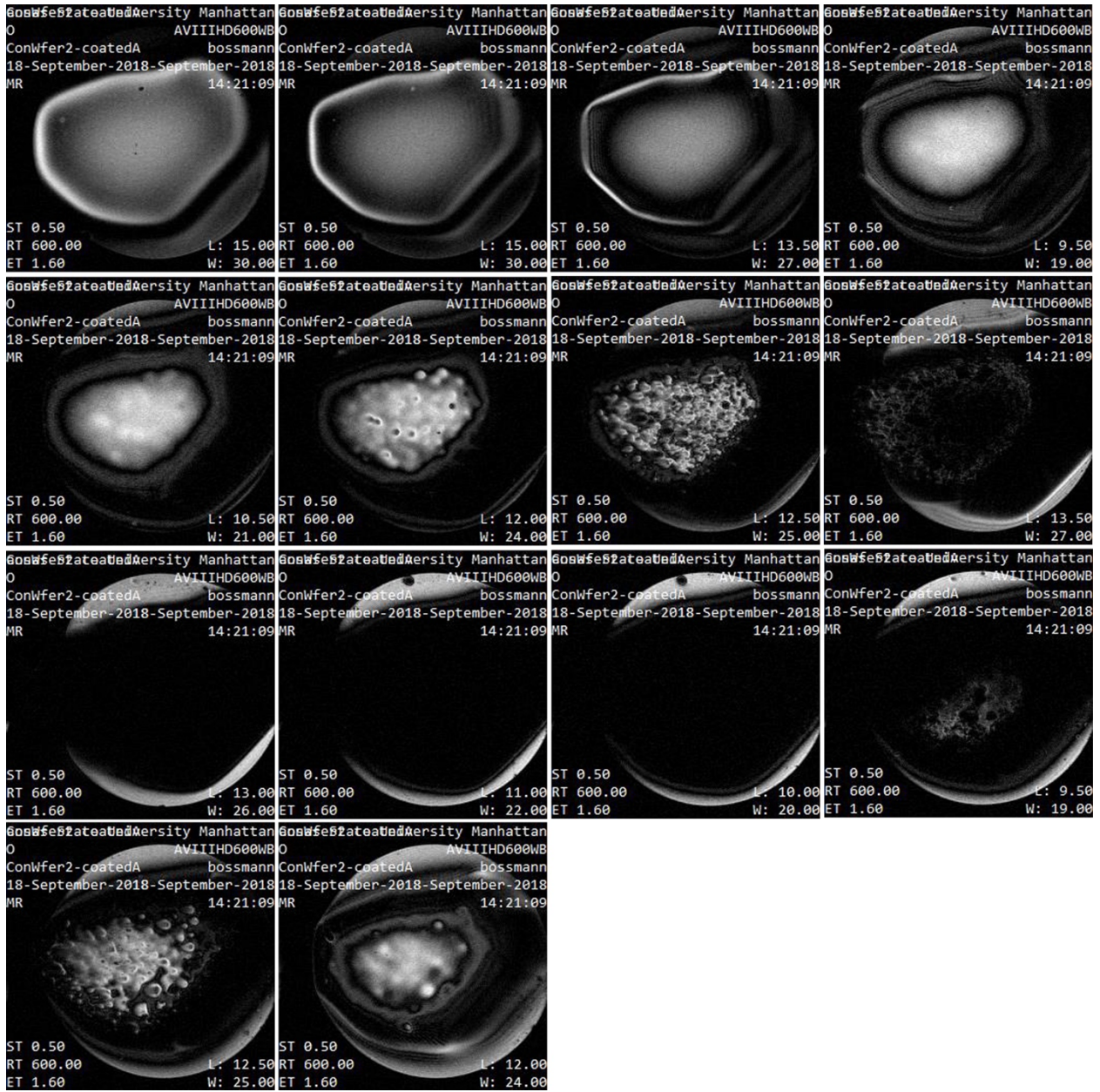
**Figure 5.10: Magnetic Resonance Imaging (MRI) of a polyepoxyamine resin (A) on the surface of a Type 2 concrete wafer (embedded in a polyacrylate gel)**

Enlarged Slices 9, 10, 11, and 12 of Figure 5.8 are shown. Each slice has a thickness of 0.175 mm. The "slices" proceed from the upper left corner to the lower right corner. The regions at the exterior of the Type 2 wafer are bright, due to the presence of protons in the adhesive polymer coating. The interior is dark, due to the absence of protons. The transition of bright to dark regions proceeds gradually, which is indicative of complete surface coating. In the middle of Type 2 wafers, imperfections (visible as grainy structures) can be discerned.
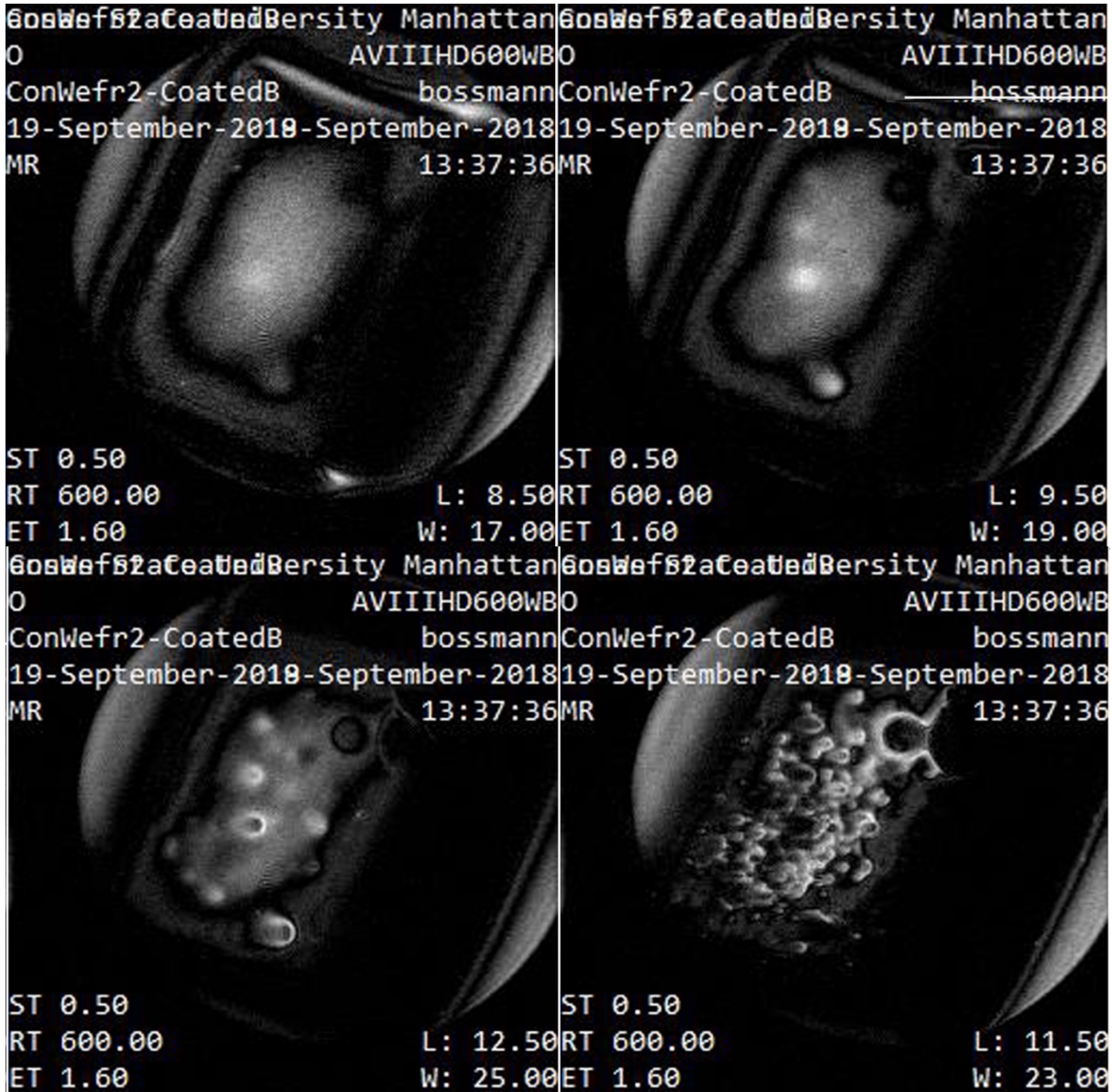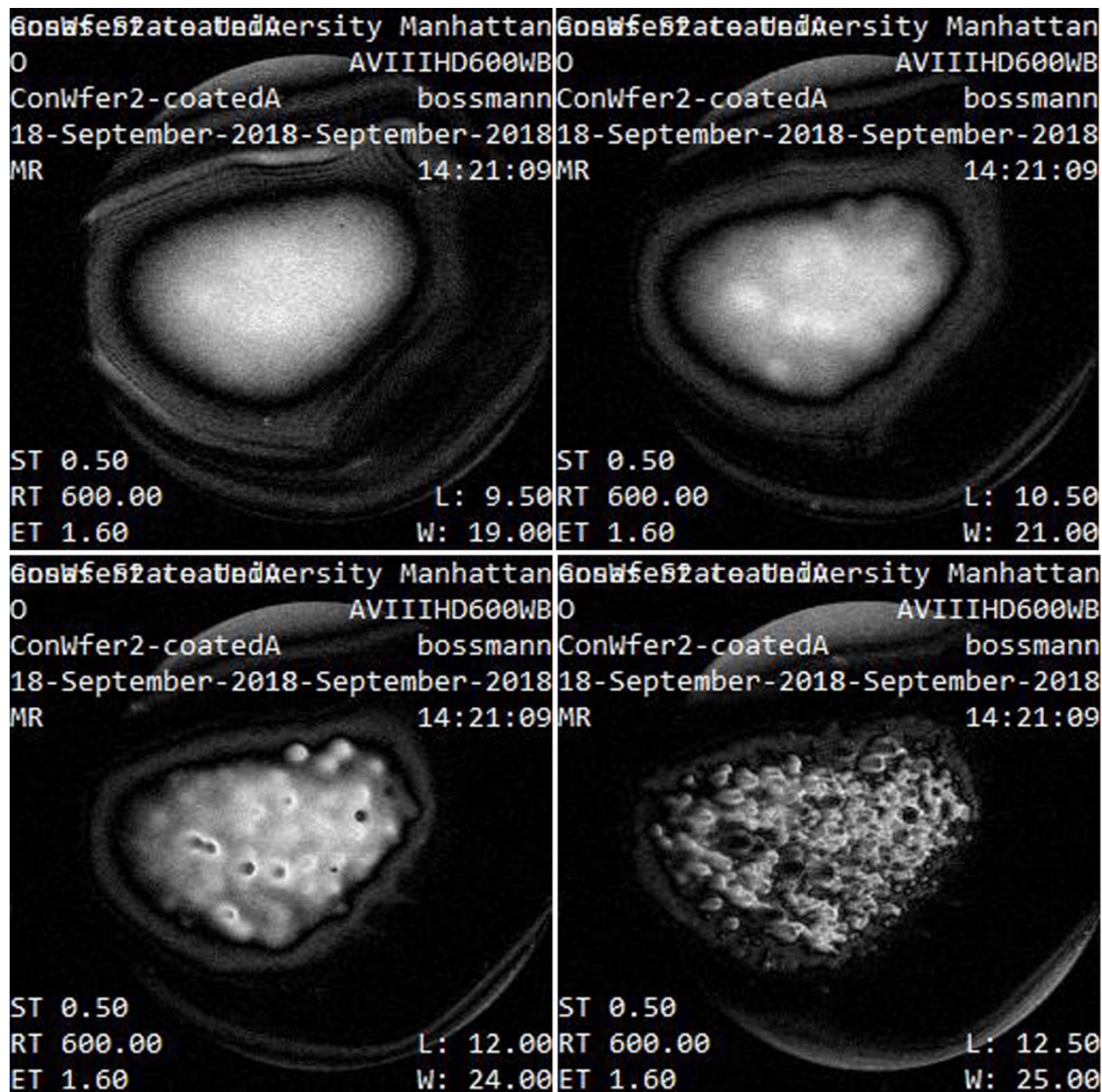
**Figure 5.11: Magnetic Resonance Imaging (MRI) of a polyepoxyamine resin (A) on the surface of a Type 2 concrete wafer (embedded in a polyacrylate gel)**
Enlarged Slices 4, 5, 6, and 7 of Figure 5.10 are shown. Each slice has a thickness of 0.175 mm. The transition from the polymer-covered surface to the interior of the wafer is shown. These images are supportive of the presence of stones with water-adsorbed (light) surfaces within the Type 2 concrete wafer's structure.

## 5.3 Summary of Phase 3

In Phase 3 of this Kansas Department of Transportation (KDOT) funded research endeavor, the Bossmann group at Kansas State University has performed the atomic force microscopy (AFM) and magnetic resonance imaging (MRI) characterization of coated and uncoated concrete wafers that were provided by KDOT. Reactive coating was performed with a polyisocyanate resin (A) and a polyepoxyamine resin (B). The use of polyisocyanate/ polyepoxyamine co-resins was abandoned, despite their superior thermal stability, because they did not adhere smoothly to concrete wafer surfaces.

It has been established by AFM that Type 1 concrete wafers provided by KDOT have a surface roughness of $\pm$ 100 nm, which must be regarded as very smooth. Type 2 concrete wafers that were made from cement paste feature a significantly larger surface roughness ($\pm$ 1000 nm). Both polyisocyanate model resin (A) and the polyepoxide model resin (B) were able to significantly smooth the (Type 2) wafers' surfaces. Polyepoxide model resin (B) performed better than polyisocyanate model resin (A).

MRI characterization of both wafer types indicates the presence of air and water bubbles, which are more pronounced in Type 2 wafers. Type 1 wafers show an inferior MRI signal-to-noise-ratio, most likely due to the presence of paramagnetic cations in the material.

Coating of Type 2 wafers with both polyisocyanate model resin (A) and the polyepoxide model resin (B) led to smoothly coated surfaces, in agreement with the AFM findings. Polyepoxide model resin (B) performed better than polyisocyanate model resin (A). In both types of coated wafers, air and—more importantly—water bubbles were present below the coatings. It is the assumption of the research team that they are already present in the wafers. It would be desirable to study the chemical binding of Resin (A) and Resin (B) in wafers that do not exhibit these structural defects. This would provide enhanced insight into the binding mechanisms of Resins (A) and (B) to concrete.

# Chapter 6: Magnetic Resonance Imaging Investigations of Untreated and (Composite) Polymer Treated Concrete Model Wafers (Provided by KDOT)

**Phase 4:** Further investigation of potential interactions of **polyepoxy/polyisocyanate composite co-resins** with the surfaces of concrete model wafers provided by KDOT in comparison with a **polyepoxy resin and** a **polyisocyanate composite resin.** Reported here are the additional results of the **magnetic resonance imaging** experiments with uncoated and coated concrete model wafers.

All MRI Pulse Sequences that have been utilized for studying the resin-covered concrete wafers have been developed by Bruker Biospin (Tang et al., 2015). As already explained, the principal advantage of using a 14.1T $B_0$ field is that according to Boltzmann statistics, the difference between the populations of parallel and antiparallel spins increases with magnetic field strength ($B_0$), leading to signal-to-noise enhancement and the requirement of shorter acquisition times for image-guided therapy (Heidemann et al., 2006). The greatest challenge of using high fields for MRI imaging is that T1 relaxation times (longitudinal magnetization recovery) increase with $B_0$, whereas T2 (transverse magnetization decay) decreases. The effects of modifications in relaxation times are such that sequences have to be adjusted to comply with slower longitudinal relaxation, shortened TE (echo time) due to reduced T2, to restore a significant T1 contrast (Inversion, MDEFT: modified driven equilibrium Fourier-transform).

The optimization of the MRI imaging procedures was performed from November 2018 to March 2019. Three conceptually different pulse sequences have been compared: FLASH (fast low angle shot magnetic resonance imaging), RARE (rapid imaging with refocused echoes), and TurboRARE, which is a faster alternative to RARE (Tang et al., 2015).

## 6.1 FLASH Sequences

FLASH sequences produce signals called gradient echo with low flip angles. They can either incorporate or completely remove the effects of transverse coherence, respectively. Here, the latter was chosen. For this purpose, FLASH uses a semi-random spoiler gradient after each echo to cause a spatially dependent phase shift. FLASH sequences are capable of generating very high T1 contrasts while suppressing susceptibility artifacts. For the purpose of characterizing the Type 2 wafers, proton densities were recorded. The results are shown in Figures 6.1a, 6.1b, and 6.1c for an untreated Type 2 concrete wafer.

## 6.1.1 FLASH Imaging of Type 2 Concrete Wafer

Note that each "slice" has a thickness of 0.175 mm.



**Figure 6.1a: Magnetic Resonance Imaging (MRI) of a Type 2 concrete wafer (embedded in a polyacrylate gel)**

The MRI contrast (FLASH sequence) is visualizing mobile water within the wafer's structure. The "slices" proceed from the upper left corner to the lower right corner. Each slice is numbered and has a thickness of 0.175 mm. An external light (= proton rich) surface is discernible, as well as numerous "inner surfaces." They consist of stones of various sizes that feature water-rich surfaces. These stones are embedded by uniform material, which is dark, due to the virtual absence of protons.

**Figure 6.1b: Magnetic Resonance Imaging (MRI) of a Type 2 concrete wafer (embedded in a polyacrylate gel)**

The MRI contrast (FLASH sequence) is visualizing mobile water within the wafer's structure. The "slices" proceed from the upper left corner to the lower right corner. Each slice is numbered and has a thickness of 0.175 mm. An external light (= proton rich) surface is discernible, as well as numerous "inner surfaces." The consist of stones of various sizes that feature water-rich surfaces. These stones are embedded by uniform material, which is dark, due to the virtual absence of protons.
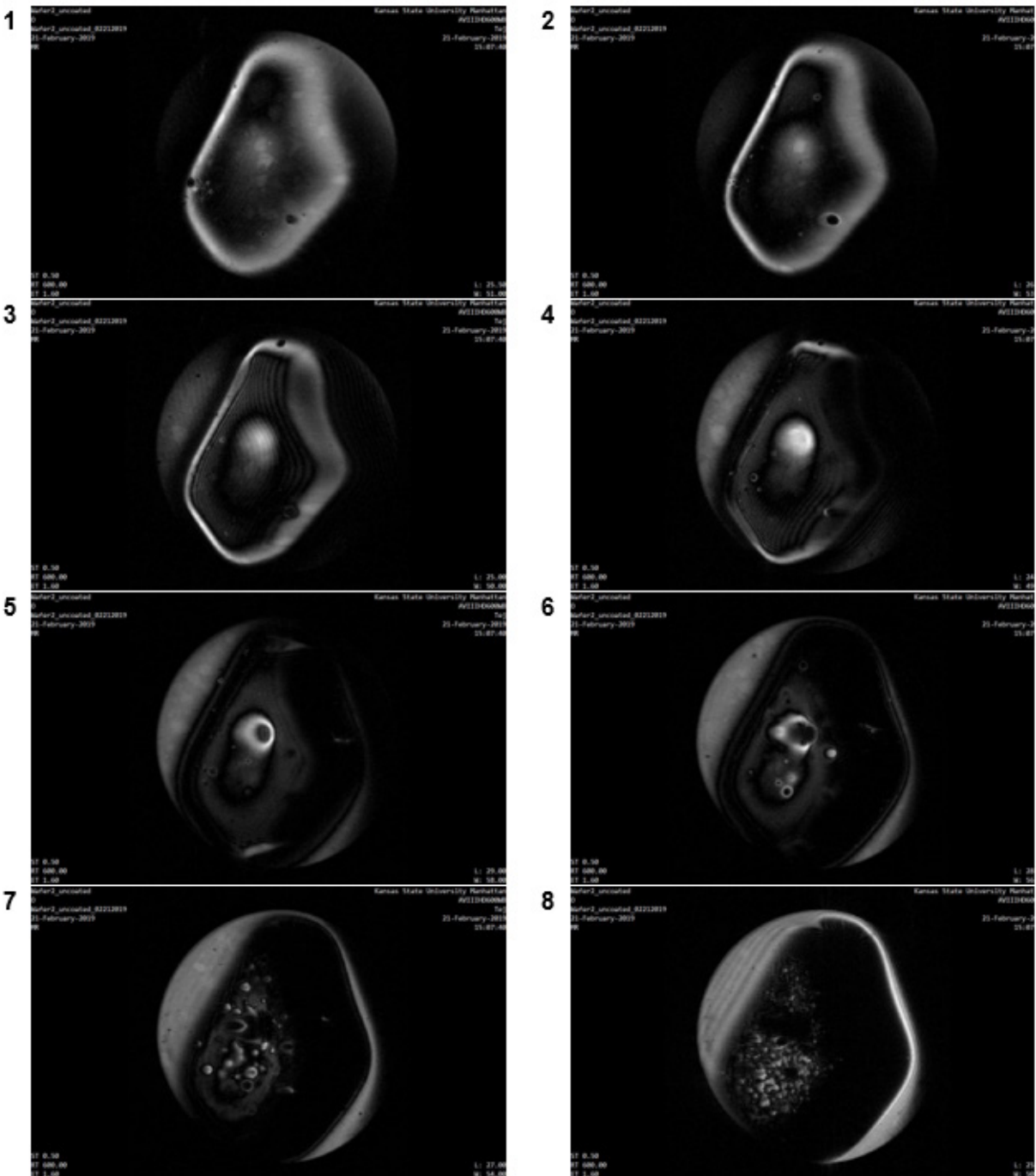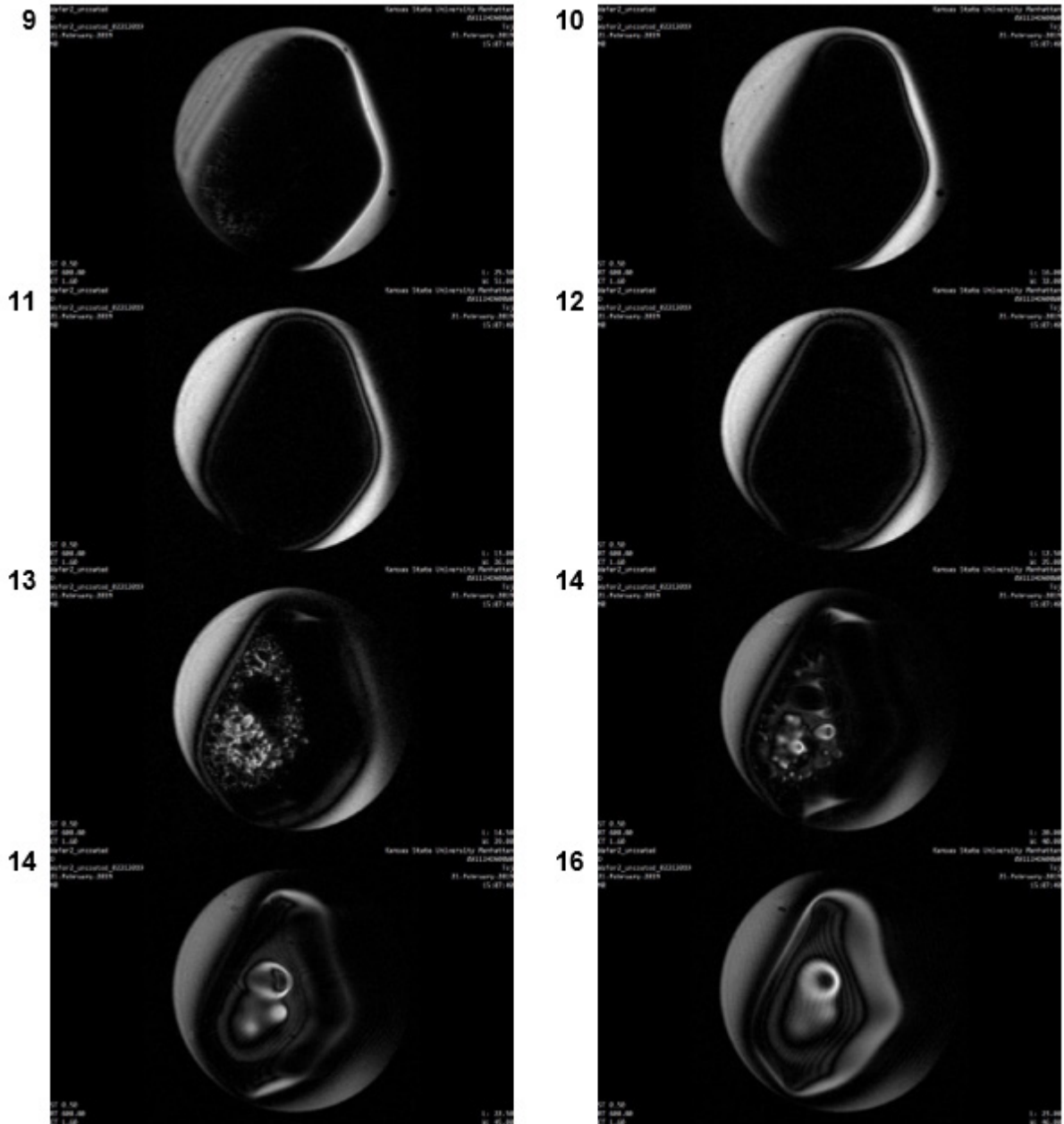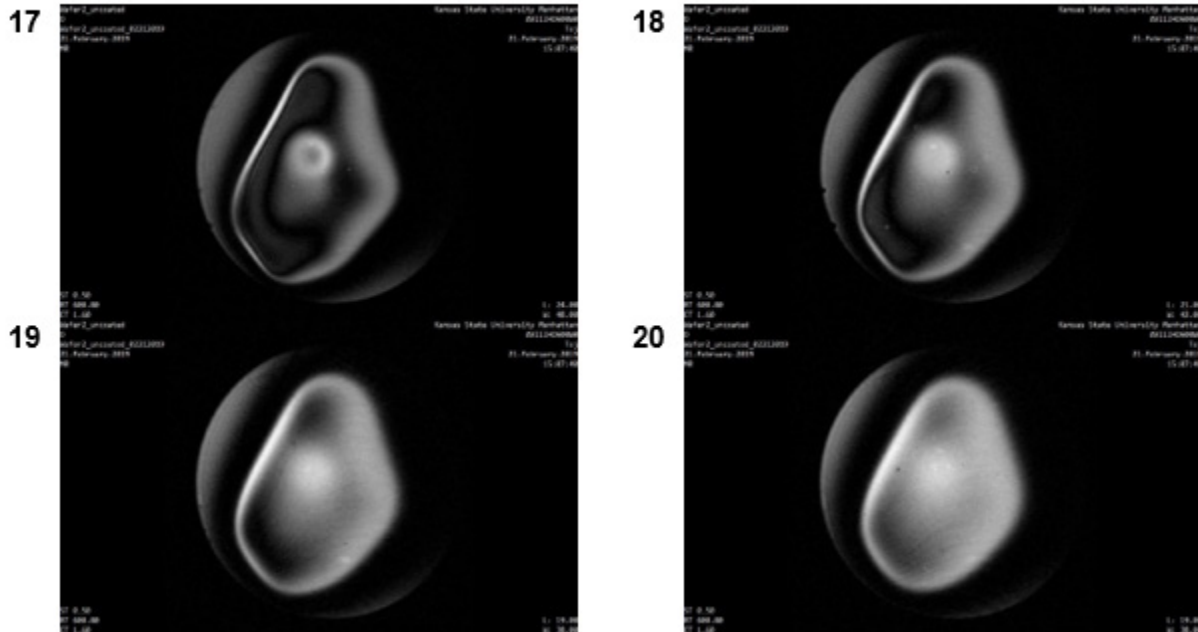
**Figure 6.1c: Magnetic Resonance Imaging (MRI) of a Type 2 concrete wafer (embedded in a polyacrylate gel)**

The MRI contrast (FLASH sequence) is visualizing mobile water within the wafer's structure. The "slices" proceed from the upper left corner to the lower right corner. Each slice is numbered and has a thickness of 0.175 mm. These images focus on the interface region between Type 2 concrete wafer and the water-rich polyacrylate gel. The surface is smooth and regular, which is ideal for polymer-adsorption experiments.

The FLASH imaging of a Type 2 concrete wafer shows smooth surfaces (Slices 1, 2 and 19, 20), which are, principally, capable of binding with polyepoxyamine resins. However, water-rich regions are discernible under the surface (Slices 3–8 and 13–18). Interestingly, the core region of the Type 2 wafer (Slices 9–12) consists of massive concrete without discernible defects. The water-rich regions are recognizable, because there, water has a higher mobility than in the surrounding concrete. They consist of the interface of stones that are embedded in the concrete matrix with the matrix itself. The chemical binding process of concrete to silanol groups at the surface of the stones is incomplete. Otherwise, suitable diffusion conditions for water would not exist. On the basis of this finding, it was concluded that the areas around stones in concrete are weakening the overall material strength, due to incomplete chemical interfacing. Furthermore, the water is evenly distributed at the surface of the Type 2 concrete wafers, indicating that very similar chemical conditions exist everywhere at the wafer's surface, making them suitable materials for coating with polyepoxyamine resins.

## 6.1.2 FLASH Imaging of Polyepoxyamine Resin (B)-coated Type 2 Concrete Wafer

Note that each "slice" has a thickness of 0.175 mm.



**Figure 6.2a: Magnetic Resonance Imaging (MRI) of a polyepoxyamine resin (B)-coated Type 2 concrete wafer (embedded in a polyacrylate gel)**

The MRI contrast (FLASH sequence) is visualizing mobile water within the wafer's structure. The "slices" proceed from the upper left corner to the lower right corner. Each slice is numbered and has a thickness of 0.175 mm. A gradual transition from proton-rich (light) polymer coating to wafer surface is shown, which is indicative of a successful coating process.

**Figure 6.2b: Magnetic Resonance Imaging (MRI) of a polyepoxyamine resin (B)-coated Type 2 concrete wafer (embedded in a polyacrylate gel)**

The MRI contrast (FLASH sequence) is visualizing mobile water within the wafer's structure. The "slices" proceed from the upper left corner to the lower right corner. Each slice is numbered and has a thickness of 0.175 mm. These images show the regions below the polymer coating and the wafer surface. After passing through a region (first 4 slices) that is characterized by the presence of embedded stones, the interior of the wafer is shown (last 4 slices), which is uniformly dark due to the absence of protons.
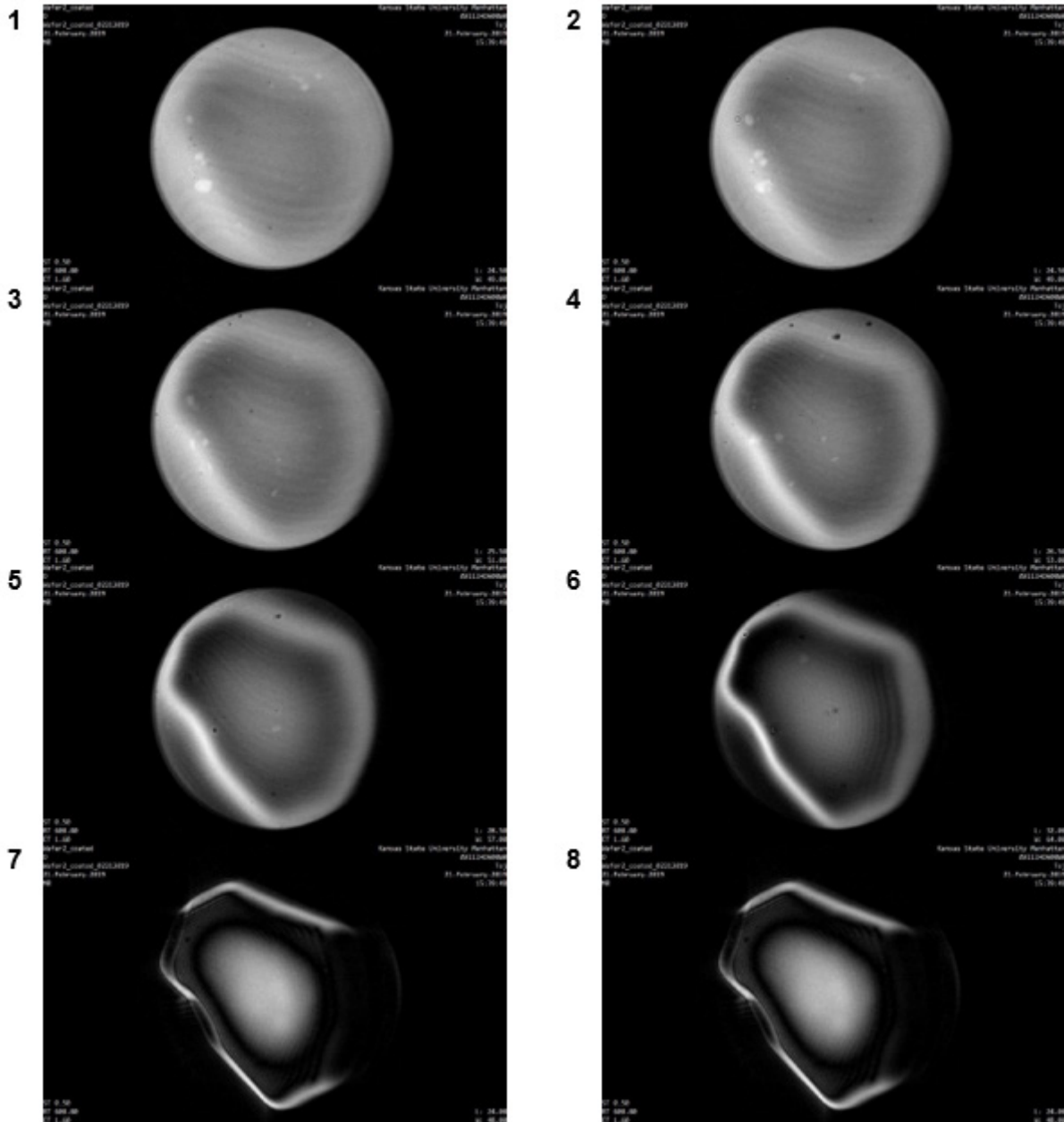
**Figure 6.2c: Magnetic Resonance Imaging (MRI) of a polyepoxyamine resin (B)-coated Type 2 concrete wafer (embedded in a polyacrylate gel)**

The MRI contrast (FLASH sequence) is visualizing mobile water within the wafer's structure. The "slices" proceed from the upper left corner to the lower right corner. Each slice is numbered and has a thickness of 0.175 mm. In the first three slices, the region of the embedded stones is reached again (moving further downwards), as this can be discerned by the presence of multiple little stones with bright surfaces. The last five slices show the smooth transition from the wafer surface into the polymer region again. The transition in brightness is gradual and the appearance of both, the wafer surface and the adherent polymer layer is smooth.

Whereas the interior of the Type 2 concrete wafer shown in Figures 6.2a, 6.2b, and 6.2c is very similar to the one that was imaged in Figures 6.1a, 6.1b, and 6.1c, the presence of polyepoxyamine resin (B) is clearly discernible in Slices 1–4 and 22–24. The average thickness of

the polymer layer is $0.65 \pm 0.05$ mm. From the equal statistical distribution of water within the polyepoxyamine resin layer on concrete, the research team concluded that it is very homogeneous. Furthermore, the chemical bond between polyepoxyamine resin layer and concrete wafer surface is strong and homogeneous as well, as indicated by the absence of regions of high or mobile water content between the polyepoxyamine resin and the concrete wafer surface. From the FLASH imaging experiments, it is concluded that polyepoxyamine resin (B) is a very good coating for Type 2 cement wafers.

## 6.2 (Turbo)-RARE Sequences

RARE (rapid imaging with refocused echoes), is a rapid imaging technique that speeds up image acquisition by acquiring more than one k-space line per repetition. In RARE multiple $\pi$ pulses are used to create many echoes. By applying a different phase encoding gradient to each echo, multiple k-space lines can be collected in one measurement. The speed up factor compared to a conventional spin-echo sequence is therefore equal to the number of refocusing pulses applied (i.e., using 4 refocusing pulses would result in a ×4 speed up). This speed up factor is often referred to as the echo train length, or turbo factor. The Turbo-RARE sequence that was used as well in these experiments allows for the speed up of MRI materials characterization by a factor of 16. Both the RARE and Turbo-RARE sequences used here are $T_1$-weighted. Whereas the FLASH sequence previously discussed is focused on the protons from diffusing water molecules, RARE and Turbo-RARE are especially suited to image protons that originate from the polymer coating at the surfaces of the Type 2 concrete wafers, as well as from tightly bound water molecules at the surfaces of the uncoated wafers. The results are shown in Figures 6.3a, 6.2b, and 6.2c (RARE); and Figures 6.5a, 6.5b, and 6.5c (Turbo-RARE) for uncoated Type 2 cement wafers; and Figures 6.4a, 6.4b, and 6.4c (Turbo-RARE); and Figures 6.6a, 6.6b, and 6.6c (Turbo-RARE) for polyepoxyamine resin (B)-coated Type 2 cement wafers.

### 6.2.1 RARE Imaging of Type 2 Concrete Wafer

Note that each "slice" has a thickness of 0.175 mm.

As anticipated by the choice of MRI imaging sequence, only a few structural features can be discerned in the interior of the concrete wafers, due to the absence of tightly bound water molecules. It is noteworthy that the protons in concrete without defects move too slowly to be

imaged by MRI. Depending on the imaging sequence selected, it will focus either on defects (RARE) or protons on surfaces (Figure 6.3a, 6.3b, and 6.3c) or polymer layers (Figure 6.4a, 6.4b, and 6.4c).
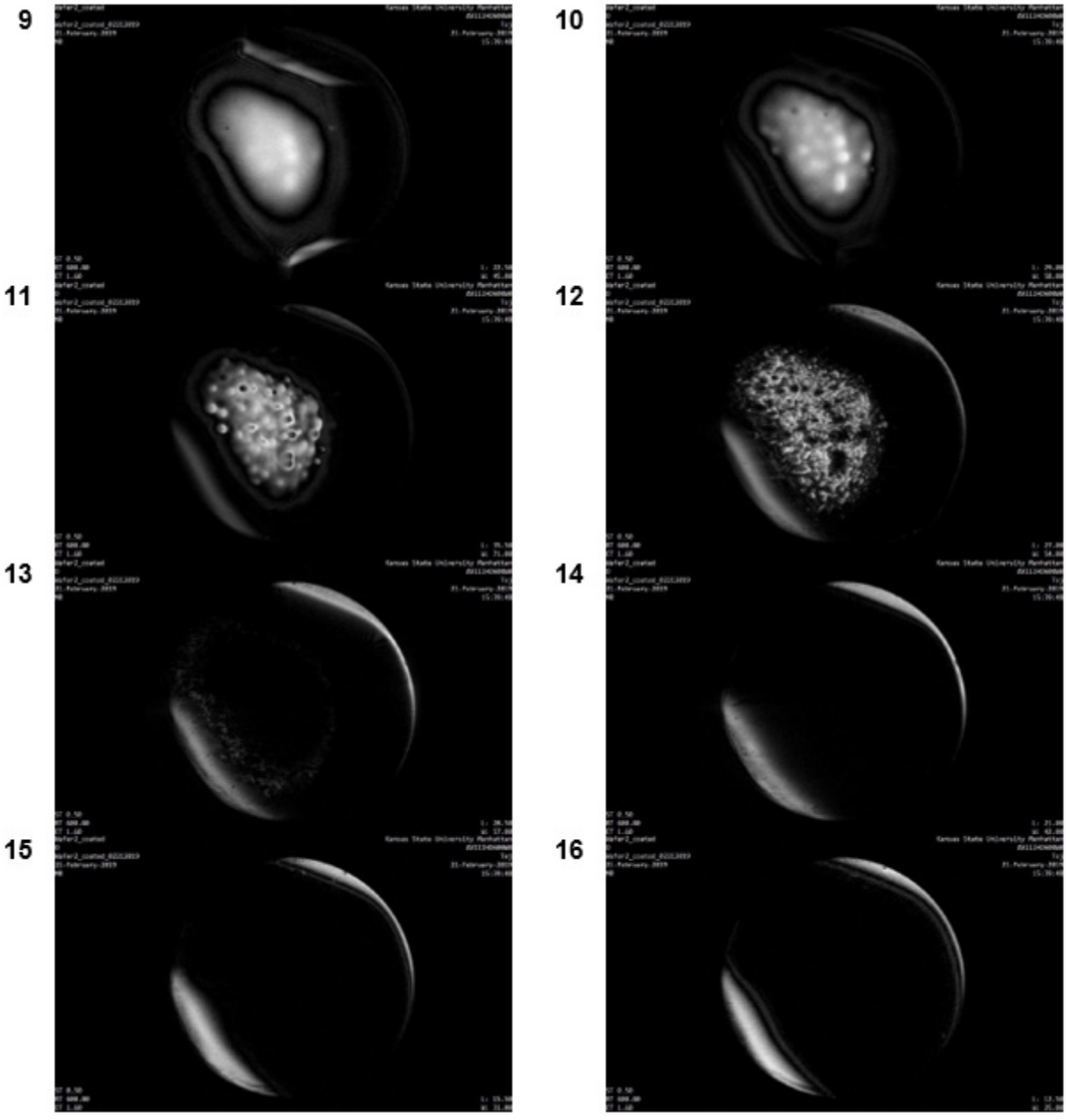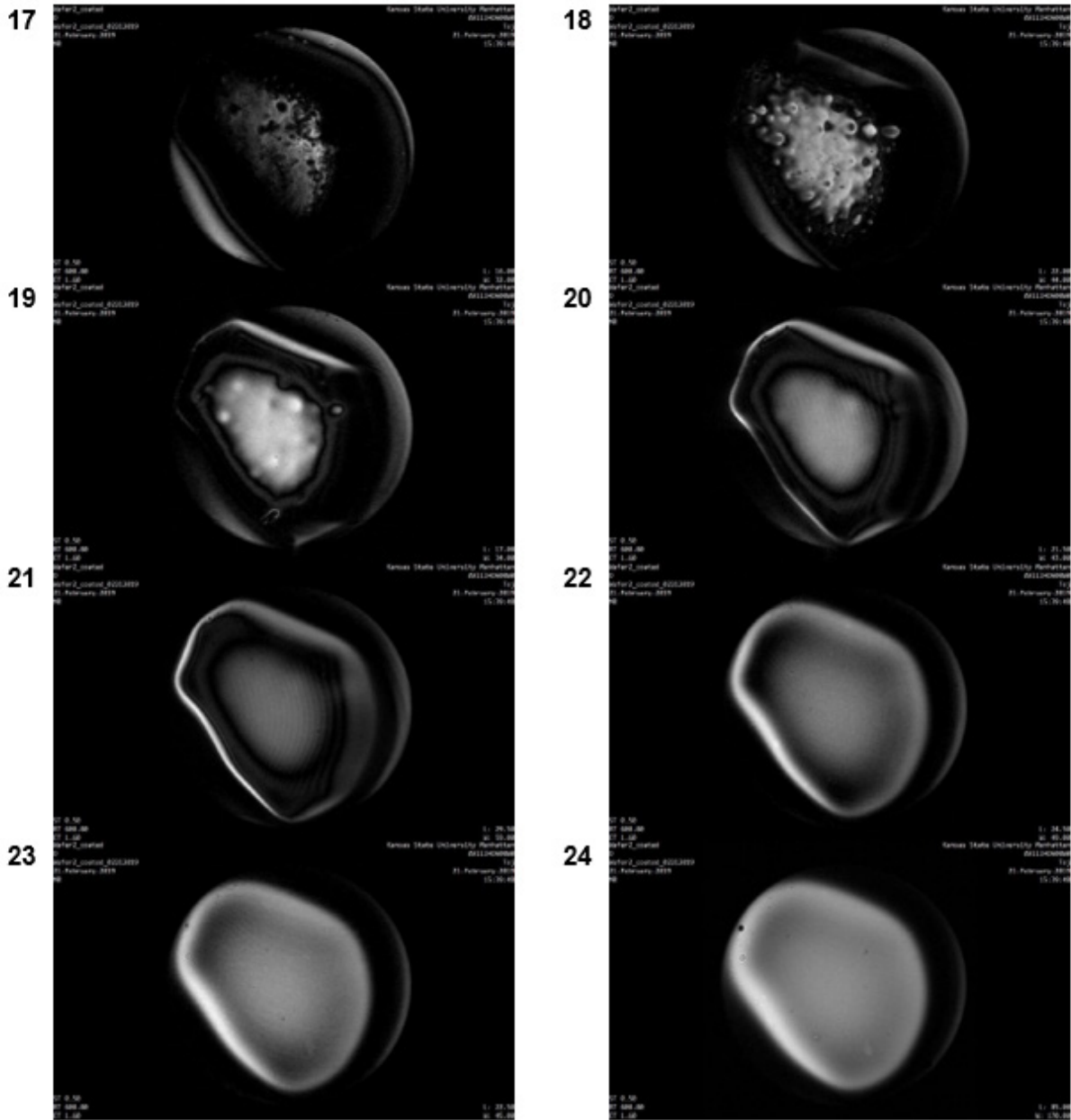


**Figure 6.3a: Magnetic Resonance Imaging (MRI) of a Type 2 concrete wafer (embedded in a polyacrylate gel)**

The MRI contrast (RARE sequence) is visualizing protons originating from tightly absorbed water at/in the wafer. The "slices" proceed from the upper left corner to the lower right corner. Each slice is numbered and has a thickness of 0.175 mm. The first four slices offer a deeper inside into the structure of the outer wafer surface. The visual appearance is "checkered," which is indicative of the presence of domains on the surface. Slices 5 to 8 show the structure of the lower wafer surface, which is almost uniform. The proton density in the surface is decreasing from slice to slice, as this is discernible from consecutive darkening. The surface of a somewhat larger stone can be seen in the middle of Slice 8 (lighter surface).

41
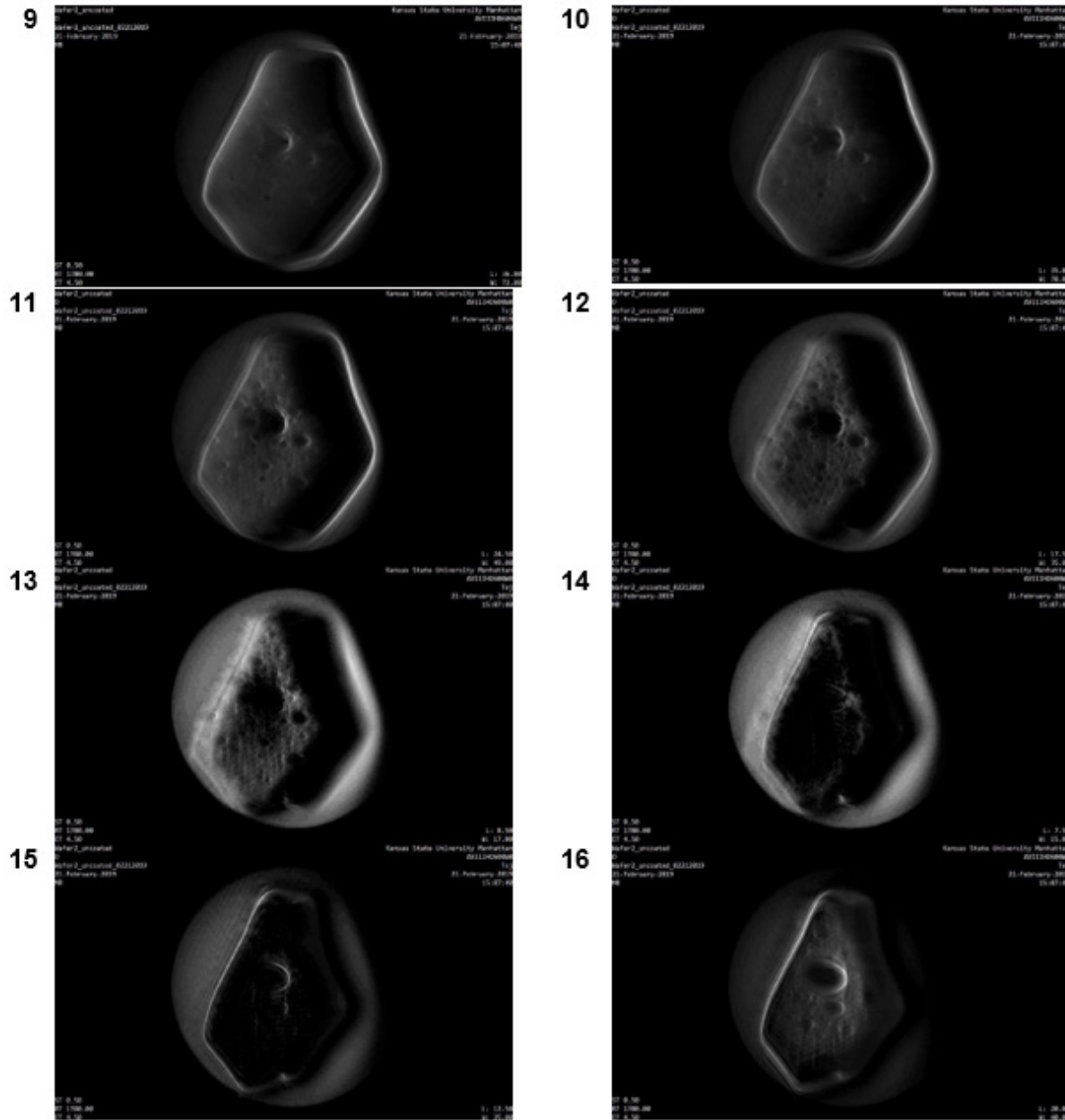
**Figure 6.3b: Magnetic Resonance Imaging (MRI) of a Type 2 concrete wafer (embedded in a polyacrylate gel)**

The MRI contrast (RARE sequence) is visualizing protons originating from tightly absorbed water at/in the wafer. The "slices" proceed from the upper left corner to the lower right corner. Each slice is numbered and has a thickness of 0.175 mm. Slices 9 to 13 show the transition from the sub-surface to the interior of the Type 2 concrete wafer. One larger stone in a central position, as well as numerous smaller stones are discernible by means of their lighter surfaces. Slices 14 to 16 show the interior of the concrete wafers. The proton density in this region is very low, resulting in dark images.
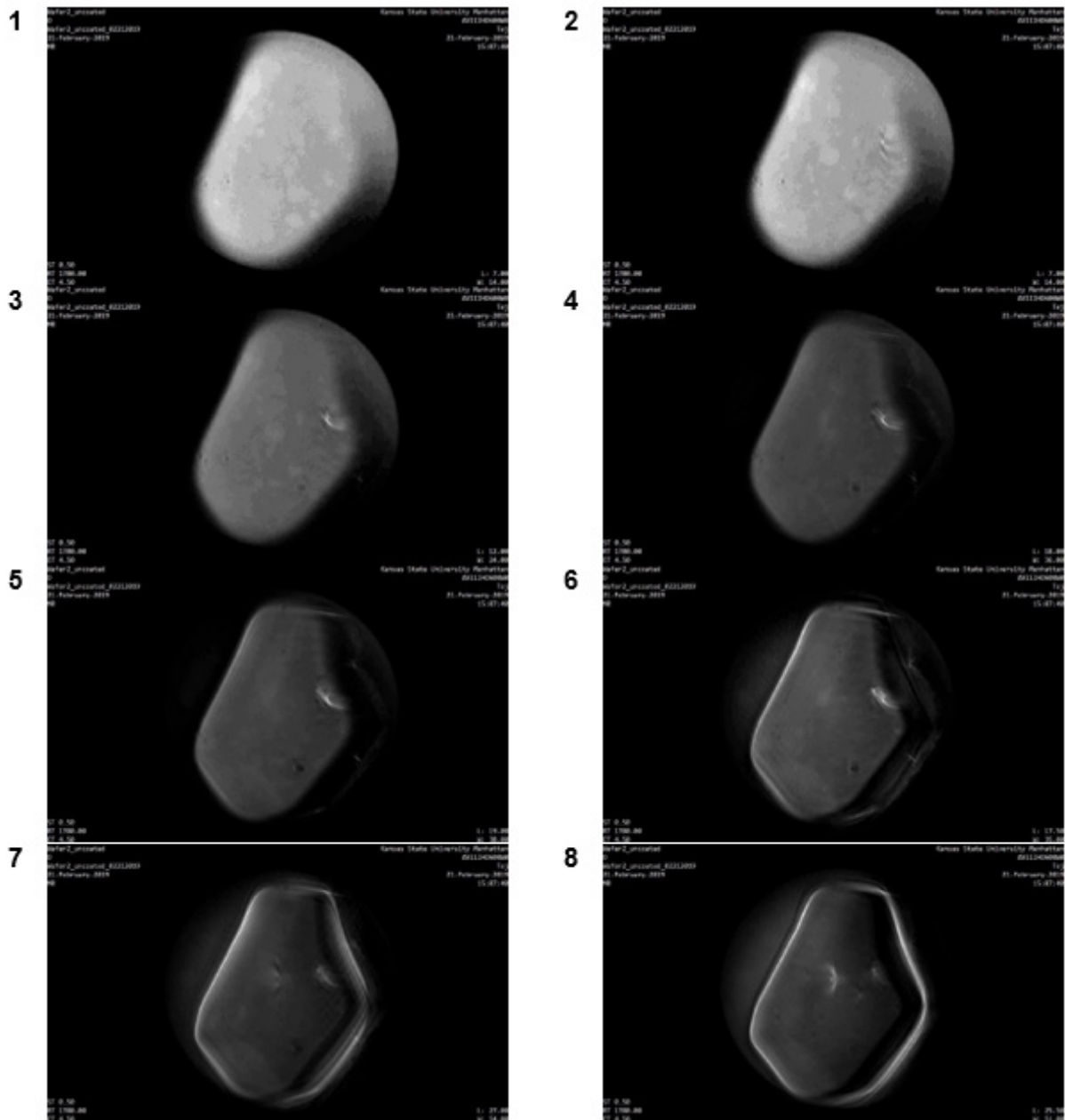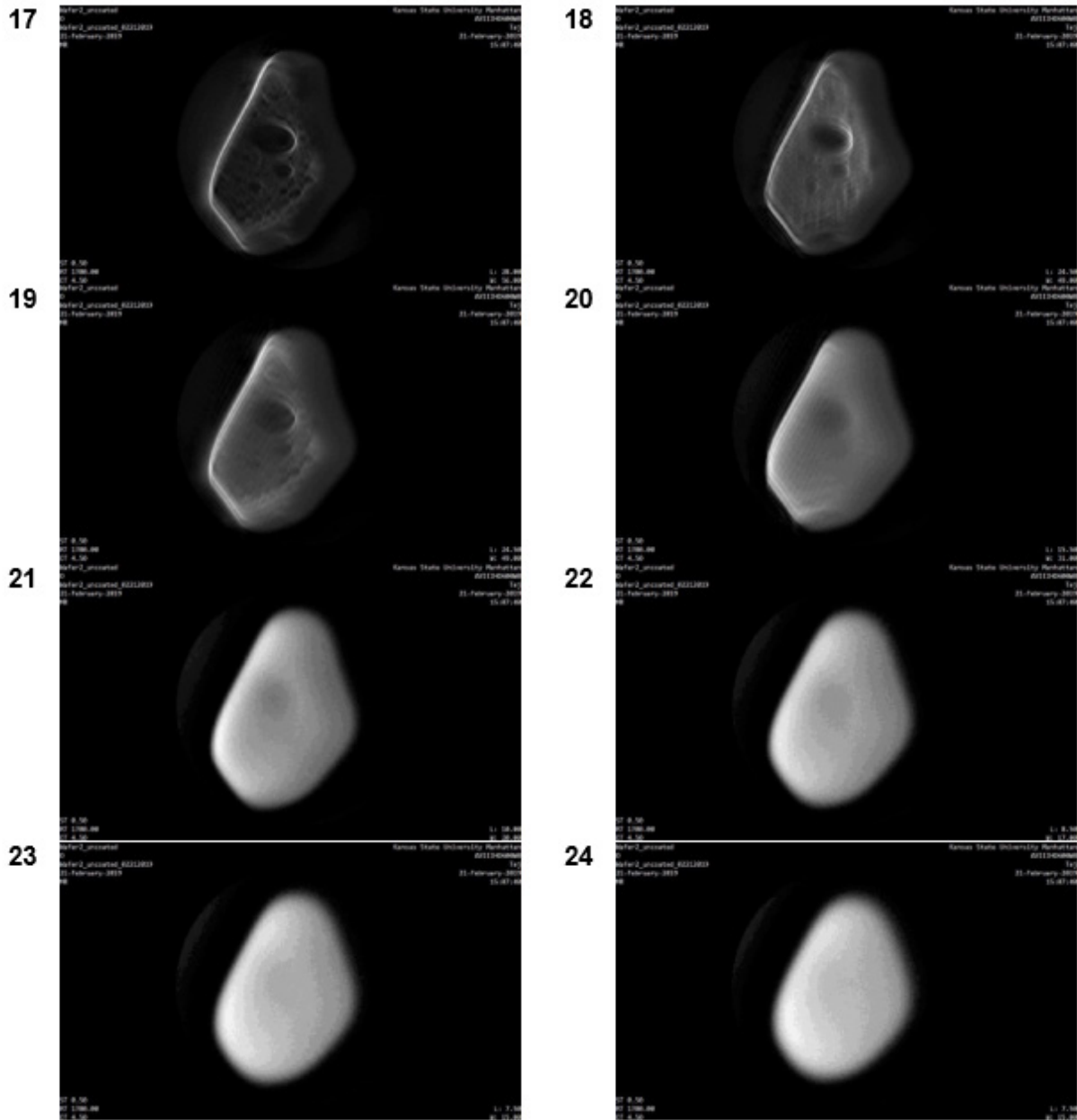
**Figure 6.3c: Magnetic Resonance Imaging (MRI) of a Type 2 concrete wafer (embedded in a polyacrylate gel)**

The MRI contrast (RARE sequence) is visualizing protons originating from tightly absorbed water at/in the wafer. The "slices" proceed from the upper left corner to the lower right corner. Each slice is numbered and has a thickness of 0.175 mm. Slices 17 to 20 show the (reverse) transition from the interior to the sub-surface region of the concrete wafer. Slices 21 to 24 show the surface region, which is characterized by the presence of domains.

From Slices 1–2 and 21–24 it is clearly discernible that the concrete interface at the surface of the wafer has a diameter of 0.5 to 0.6 mm. It is quite homogeneous, which is suitable for binding polymer resins. From a standpoint of wafer quality control, this is exactly what is anticipated for models for concrete used in infrastructure. The KDOT engineers are to be commended for developing such a suitable concrete interface.

43

## 6.2.2 RARE Imaging of Polyepoxyamine Resin (B)-coated Type 2 Concrete Wafer

Note that each "slice" has a thickness of 0.175 mm.



**Figure 6.4a: Magnetic Resonance Imaging (MRI) of a polyepoxyamine resin (B)-coated Type 2 concrete wafer (embedded in a polyacrylate gel)**

The MRI contrast (RARE sequence) is visualizing protons originating from tightly absorbed water at/in the wafer's polymer coating. The "slices" proceed from the upper left corner to the lower right corner. Each slice is numbered and has a thickness of 0.175 mm. Slices 1 to 6 show the gradual transition from the polymer-covered surface through the original wafer-surface. The appearance of the bright surface (= high proton concentration) is "checkered," which is indicative of the presence of domains. Each slice is gradually darkening, without a significant change of the general appearance. A clear boundary between polymer coating and wafer surface is not discernible, which is indicative of a very good coating. Slices 7 and 8 show the sub-surface of the Type 2 wafer, as discussed in Figures 6.3b and 6.3c.

**Figure 6.4b: Magnetic Resonance Imaging (MRI) of a polyepoxyamine resin (B)-coated Type 2 concrete wafer (embedded in a polyacrylate gel)**

The MRI contrast (RARE sequence) is visualizing protons originating from tightly absorbed water at/in the wafer's polymer coating. The "slices" proceed from the upper left corner to the lower right corner. Each slice is numbered and has a thickness of 0.175 mm. Slices 9 to 14 show the interior of the Type 2 concrete wafer. Larger and smaller stones that are embedded in the structure are discernible by means of their lighter surfaces. Slices 15 and 16 show the interior of the wafer, which are darkest, because of their lowest proton content.
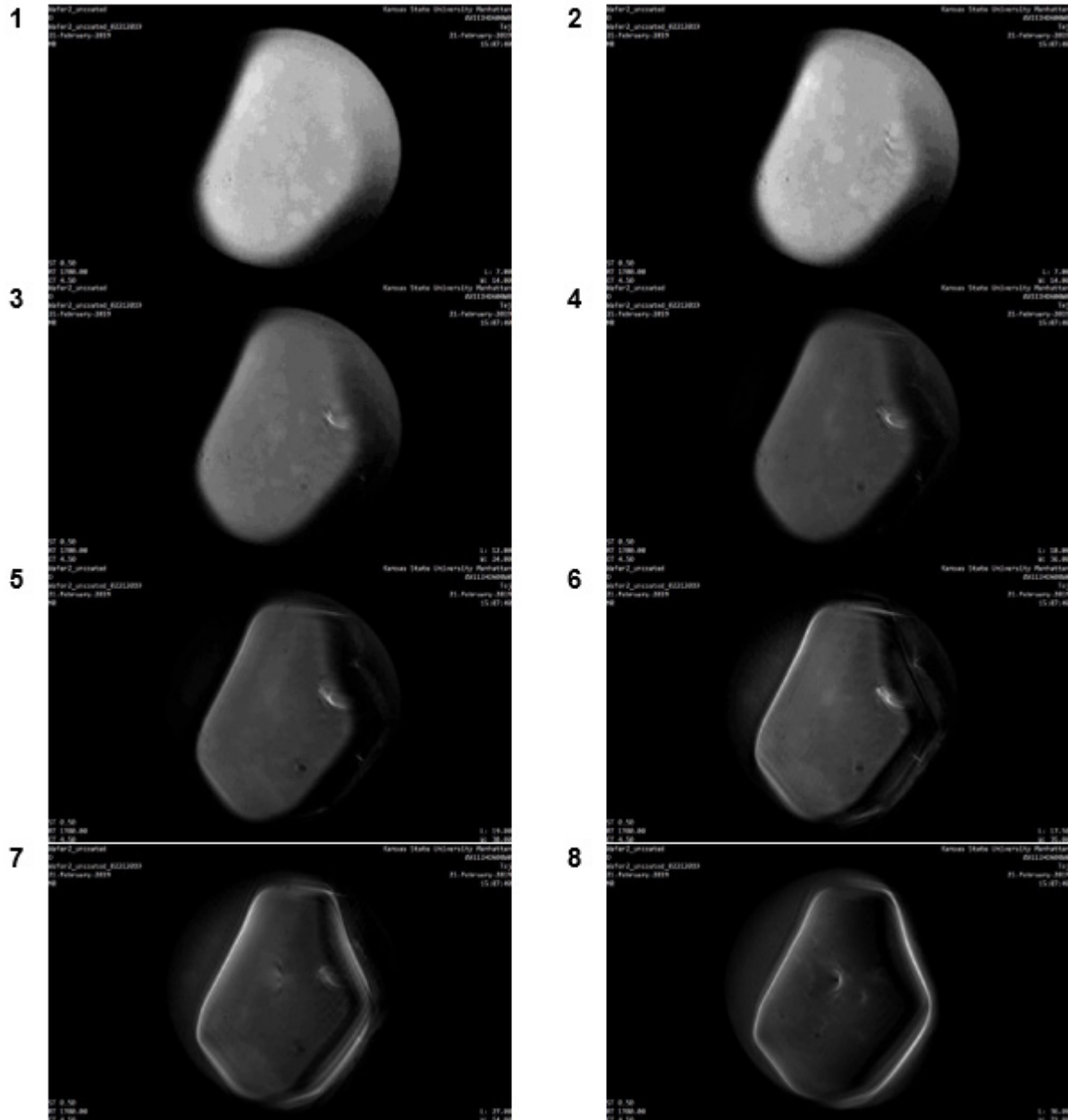
**Figure 6.4c: Magnetic Resonance Imaging (MRI) of a polyepoxyamine resin (B)-coated Type 2 concrete wafer (embedded in a polyacrylate gel)**

The MRI contrast (RARE sequence) is visualizing protons originating from tightly absorbed water at/in the wafer's polymer coating. The "slices" proceed from the upper left corner to the lower right corner. Each slice is numbered and has a thickness of 0.175 mm. Slices 17 to 19 show the (reverse) transition through the sub-surface region of the wafer. The proton content is gradually increasing, resulting in a consecutive brightening. Slices 20 to 24 show the (reverse) transition through the surface-region of the wafer and the polymer coating. A clear boundary is not discernible. A consecutive brightening is also observed here from layer to layer. The typical domain structure is visible again.

In Slices 1, 2, and 21–24 polyepoxyamine resin (B) domains on the surface of Type 2 concrete wafers can be discerned. This is typical behavior of polyepoxide polymers on surfaces (Harada, Sumitomo, Nishimoto, & Ochi, 2009), which grow in networks of integrated domains. Their sizes range from 0.2 mm in diameter to about 8 mm. It is noteworthy that the thickness of the polyepoxyamine resin (B)-coating at the surface of the Type 2 concrete wafer is about 0.5 to 0.7 mm, which is essentially the same as the thickness of the surface region of the uncoated concrete wafer. This is a clear indication that the polyepoxyamine resin (B) is filling virtually all of the pockets that exist on the concrete surface. The absence of fast-moving water (see Figures 6.2a, 6.2b, and 6.2c, FLASH imaging sequence) proves that the interfacing of concrete surface and polyepoxyamine layer is virtually perfect. This is exactly the interface that is required for applications of polymer-coatings in the transportation sector.

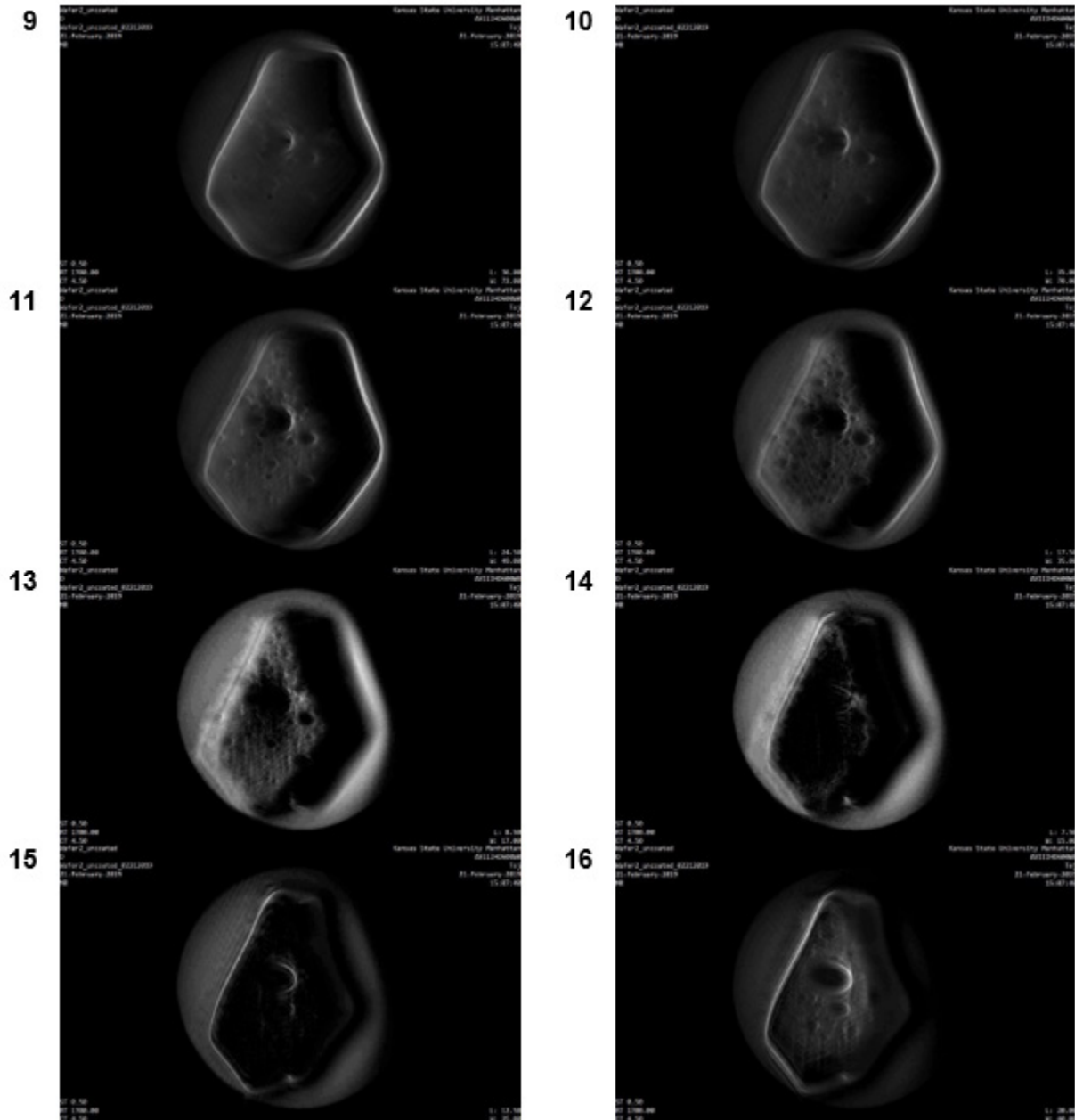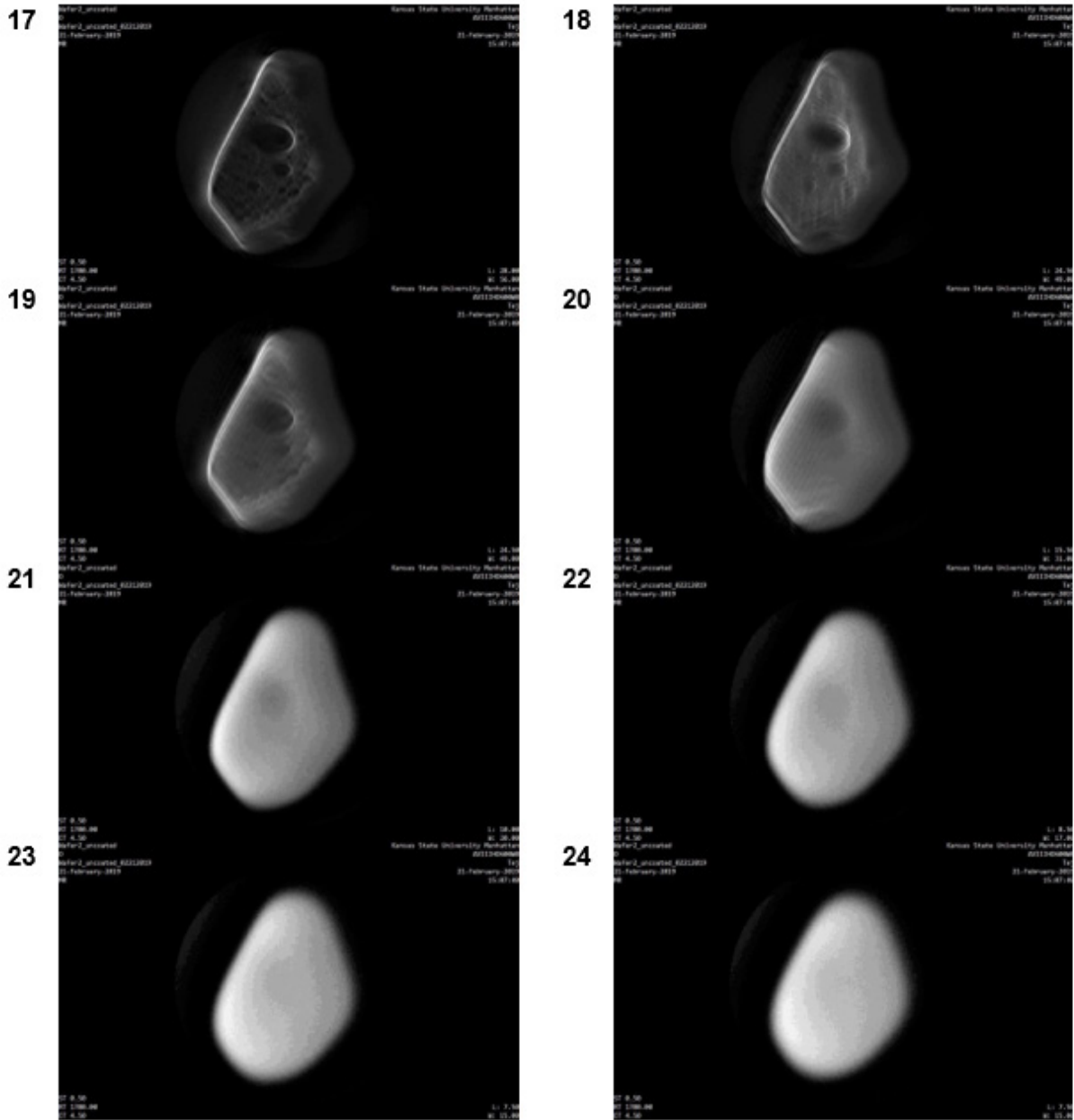## 6.2.3 Turbo-RARE Imaging of Type 2 Concrete Wafer

Note that each "slice" has a thickness of 0.175 mm.



**Figure 6.5a: Magnetic Resonance Imaging (MRI) of a Type 2 concrete wafer (embedded in a polyacrylate gel)**

The MRI contrast (Turbo-RARE sequence) is visualizing protons originating from tightly absorbed water at/in the wafer. The "slices" proceed from the upper left corner to the lower right corner. Each slice is numbered and has a thickness of 0.175 mm. Slices 1 to 5 show the surface region of the wafer surface, but with less details than when using RARE. The transition from slice to slice is gradual, but the overall signal strength is low, resulting in dark images, which don't allow the discernment of many subtleties. Slices 6 to 8 show the transition to the inner region of the wafer. Single stones become visible by means of their lighter (= proton rich) surfaces.

**Figure 6.5b: Magnetic Resonance Imaging (MRI) of a Type 2 concrete wafer (embedded in a polyacrylate gel)**

The MRI contrast (Turbo-RARE sequence) is visualizing protons originating from tightly absorbed water at/in the wafer. The "slices" proceed from the upper left corner to the lower right corner. Each slice is numbered and has a thickness of 0.175 mm. Slice 9 is still part of the transition to the inner region of the wafer. In Slices 10 to 13 the wafer's interior becomes visible. It does not feature any discernible structures and is quite homogeneous. Slices 14 and 16 show the sub-surface of the wafer. Contrast is lower than when using RARE.

The Turbo-RARE MRI imaging of the Type 2 concrete wafer (Figures 6.5a, 6.5b, 6.5c) yielded principally the same results as RARE imaging (Figures 6.3a, 6.3b, 6.3c), with the exception that it shows that the surface regions of the concrete wafers (Slices 18–24) are somewhat

more extended than visible when using RARE. From the Turbo-RARE results, it is estimated that the true diameter of this layer is closer to 1.0–1.2 mm. It appears to be very homogeneous, which clearly shows that Type 2 cement wafers are most suitable.
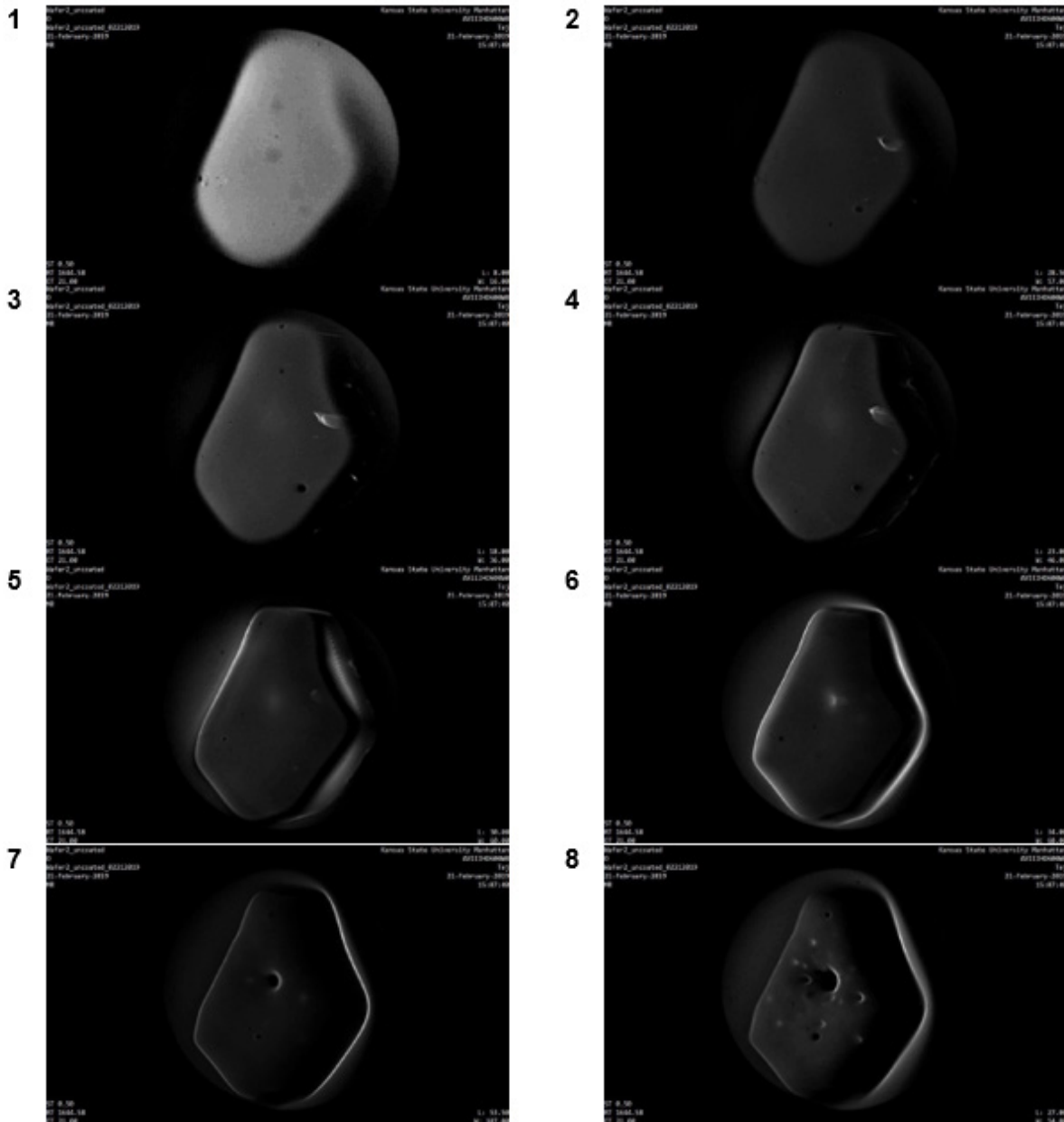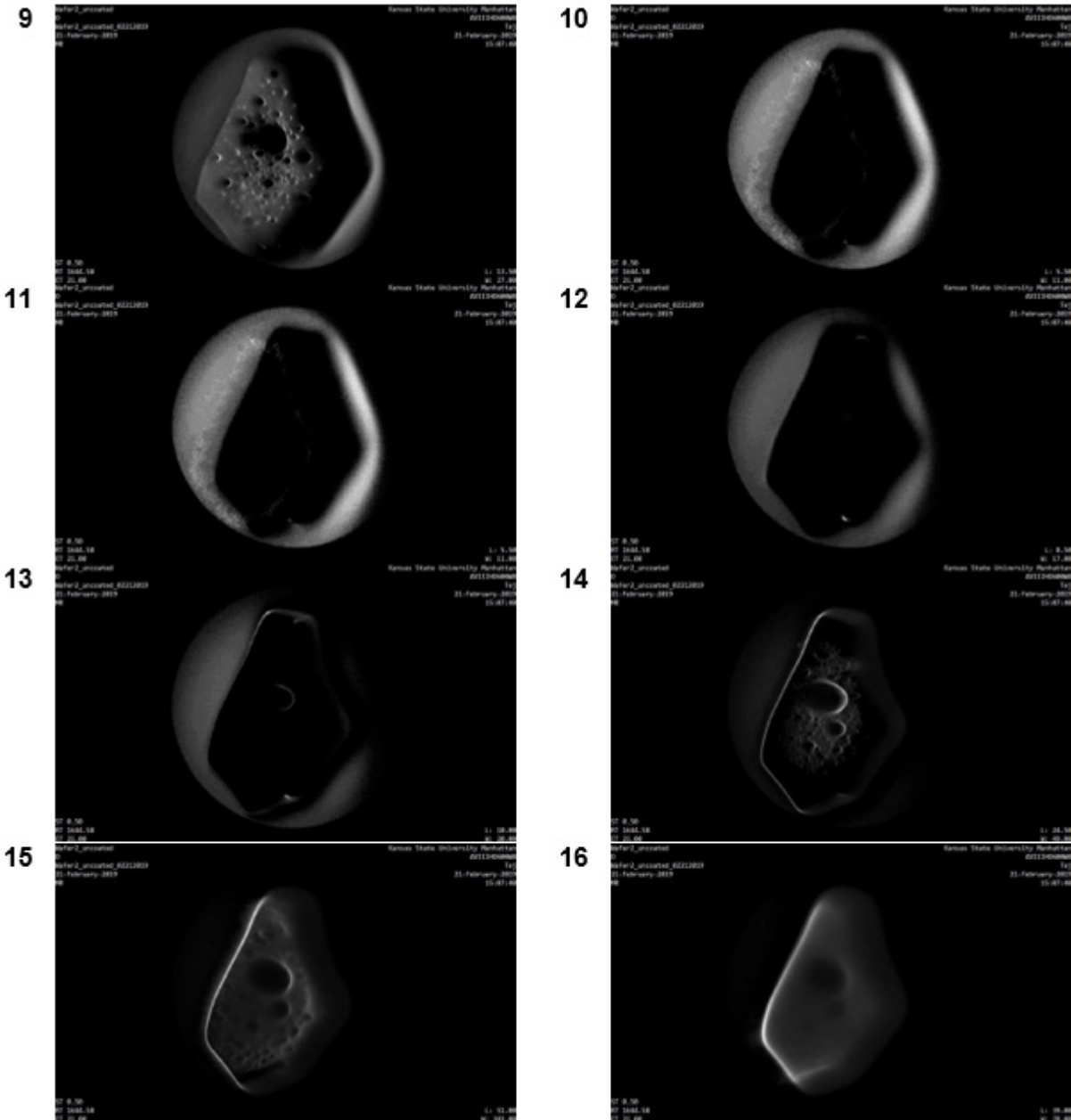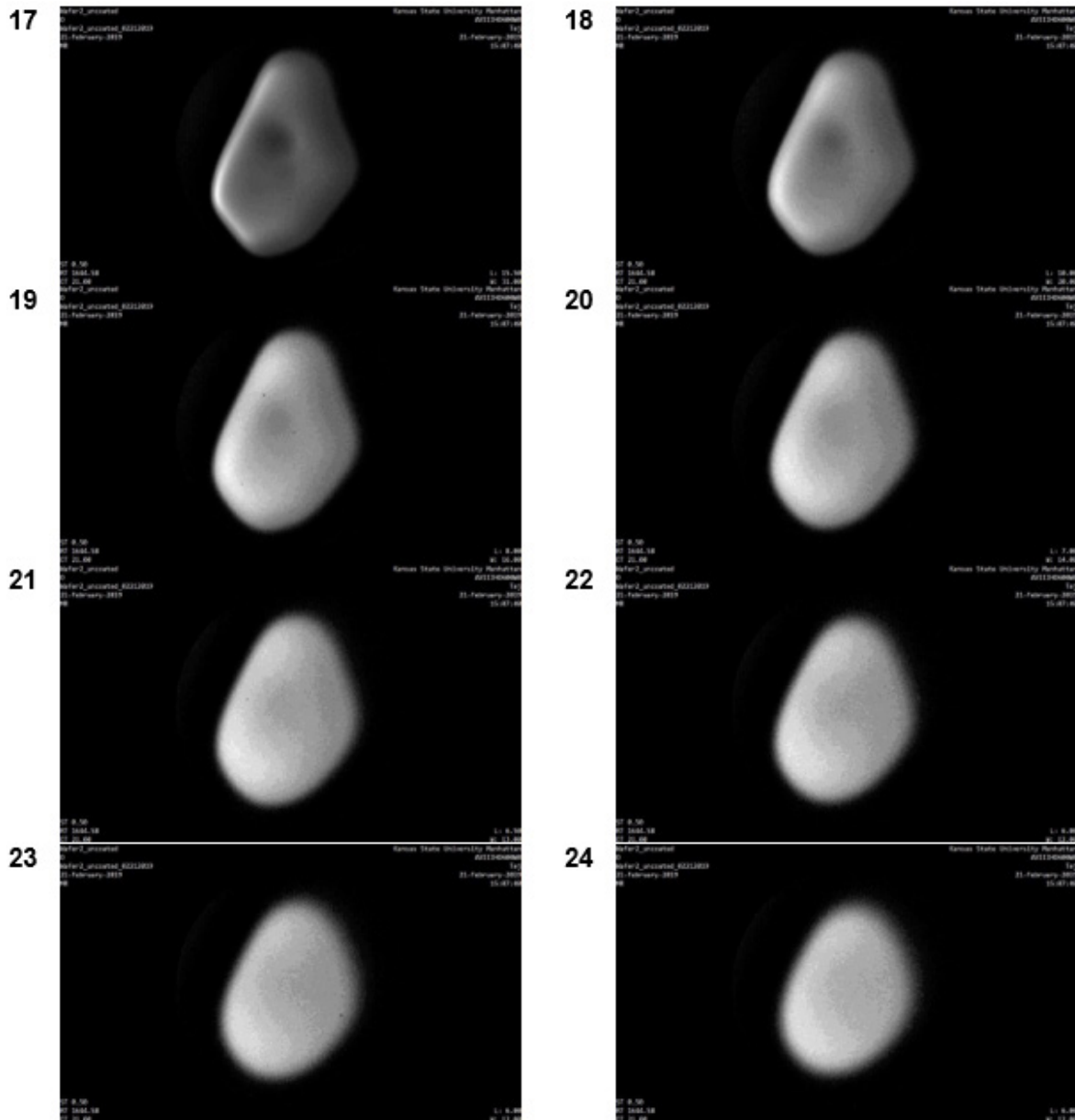


**Figure 6.5c: Magnetic Resonance Imaging (MRI) of a Type 2 concrete wafer (embedded in a polyacrylate gel)**

The MRI contrast (Turbo-RARE sequence) is visualizing protons originating from tightly absorbed water at/in the wafer. The "slices" proceed from the upper left corner to the lower right corner. Each slice is numbered and has a thickness of 0.175 mm. Slices 17 to 22 show the surface region of the wafer, which is virtually uniform (only a few domains are visible).

## 6.2.4 Turbo-RARE Imaging of Polyepoxyamine Resin (B)-coated Type 2 Concrete Wafer

Note that each "slice" has a thickness of 0.175 mm.



**Figure 6.6a: Magnetic Resonance Imaging (MRI) of a polyepoxyamine resin (B)-coated Type 2 concrete wafer (embedded in a polyacrylate gel)**

The MRI contrast (Turbo-RARE sequence) is visualizing protons originating from tightly absorbed water at/in the wafer's polymer coating. The "slices" proceed from the upper left corner to the lower right corner. Each slice is numbered and has a thickness of 0.175 mm. Slices 1 to 3 show the polymer coating on the Type 2 concrete wafer, which appears smooth and is bright due to the presence of polymer-bound protons. Slices 4 and 5 show the boundary region between polymer coating and surface (brighter band-like structure). Slices 6 and 8 show the original surface region of the concrete wafer. Since their proton content is lower than the polymer coating, they appear dark and virtually without discernible structures.
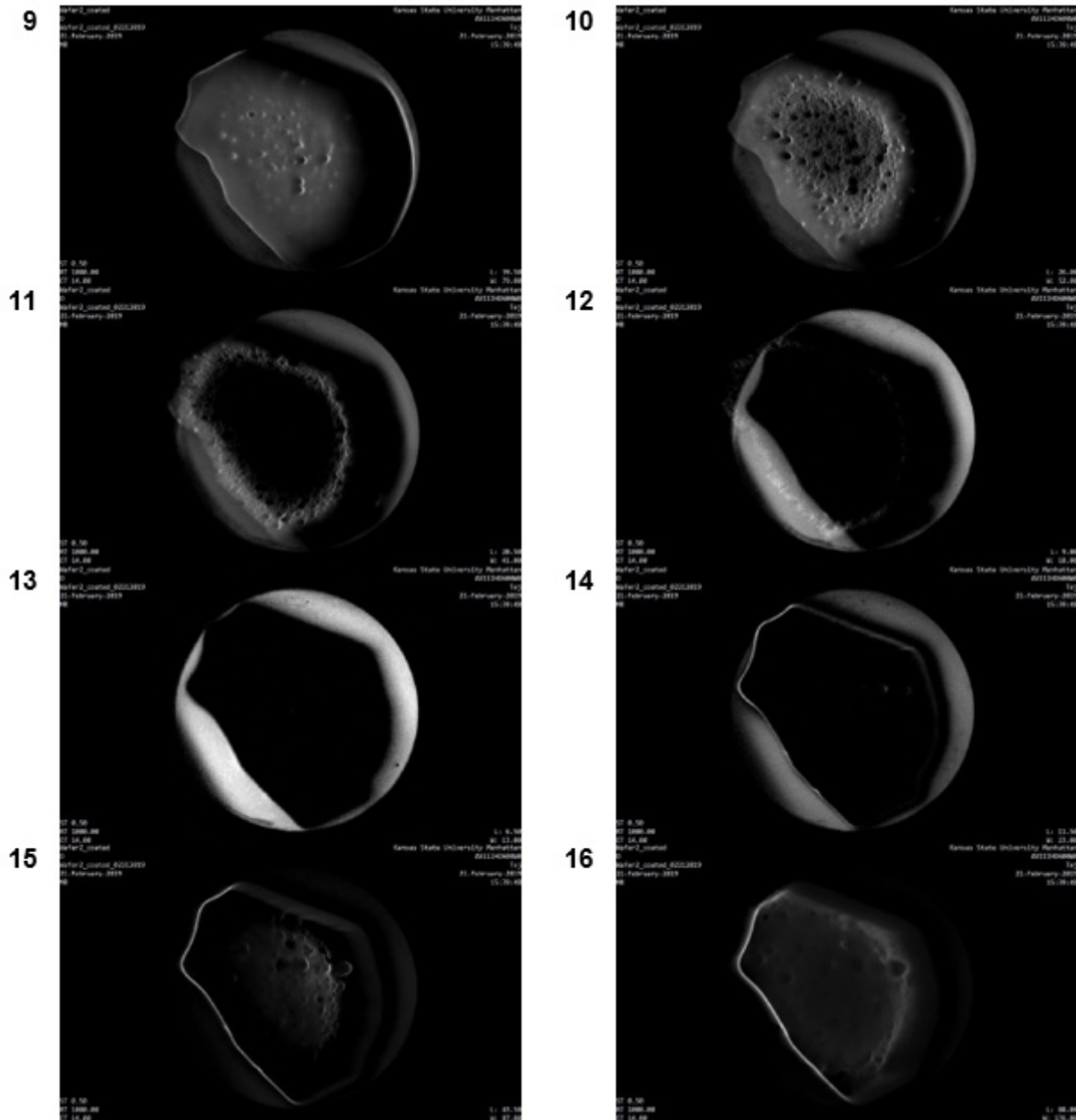
**Figure 6.6b: Magnetic Resonance Imaging (MRI) of a polyepoxyamine resin (B)-coated Type 2 concrete wafer (embedded in a polyacrylate gel)**

The MRI contrast (Turbo-RARE sequence) is visualizing protons originating from tightly absorbed water at/in the wafer's polymer coating. The "slices" proceed from the upper left corner to the lower right corner. Each slice is numbered and has a thickness of 0.175 mm. Slices 9 to 11 show the sub-surface region, which is here full of little stones (dark cores, bright surfaces). Slices 12 and 13 show the structureless interior of the wafer. Slices 15 and 16 show the (reverse) transition from the core region to the sub-surface. The presence of little stones is discernible.
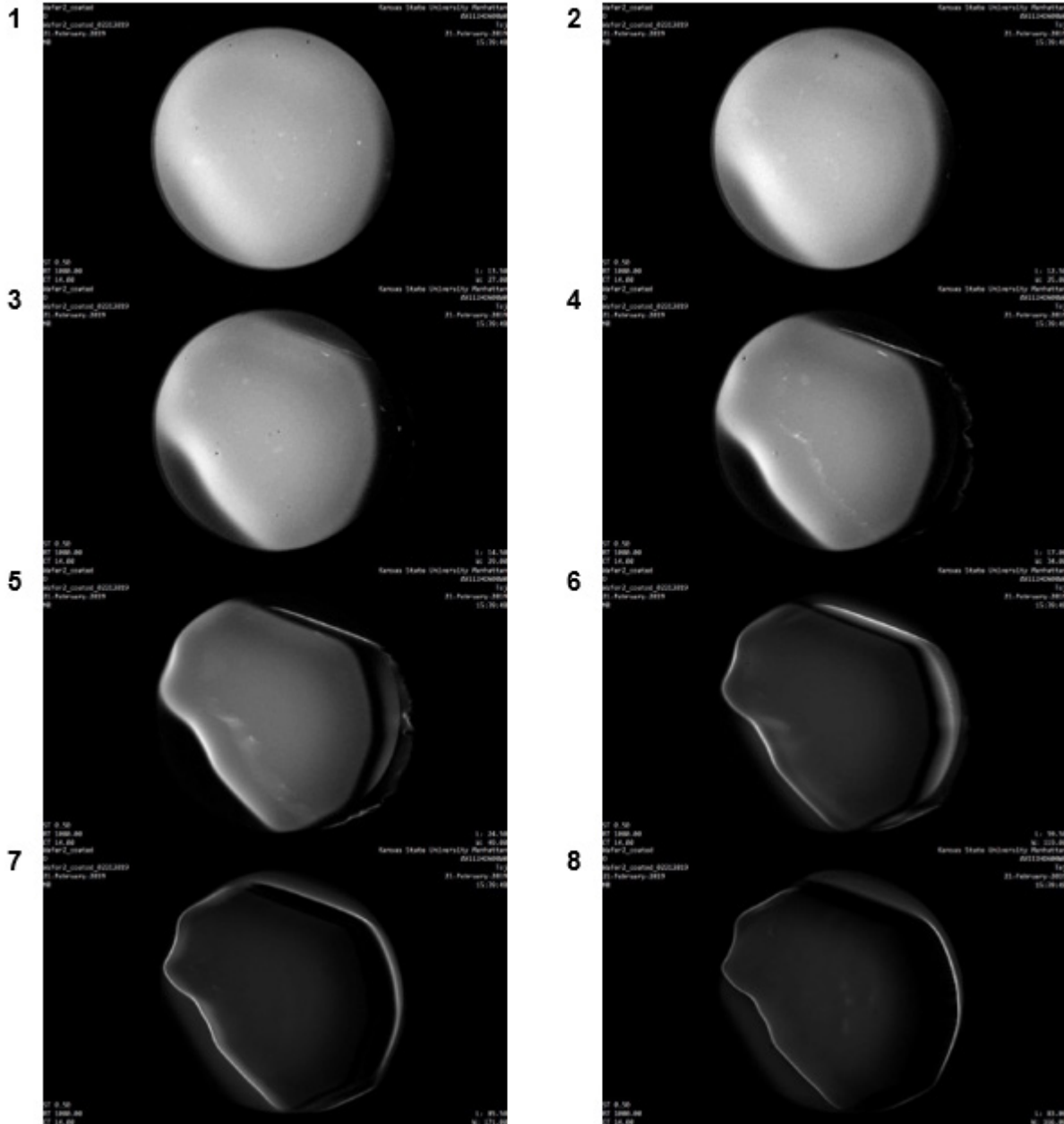
**Figure 6.6c: Magnetic Resonance Imaging (MRI) of a polyepoxyamine resin (B)-coated Type 2 concrete wafer (embedded in a polyacrylate gel)**

The MRI contrast (Turbo-RARE sequence) is visualizing protons originating from tightly absorbed water at/in the wafer's polymer coating. The "slices" proceed from the upper left corner to the lower right corner. Each slice is numbered and has a thickness of 0.175 mm. Slices 17 to 19 show the original surface of the wafer, which is smooth. Each slice increases in brightness, indicating an increasing proton content. Slice 20 shows the boundary region between the original concrete surface and the polymer coating. Here, the transition is smooth, indicating excellent adhesion. Slices 22 to 24 show the polymer coating, which is virtually without features indicating a smooth coating.

In agreement with the results obtained with uncoated Type 2 wafers using the Turbo-RARE imaging sequence, a somewhat more extended polyepoxyamine resin (B) layer on the surface of the cement wafer was found. The extension of the polymer layer is very close to the original surface region on concrete, about 1.2 mm (Slices 18–24). In analogy to the findings when using the RARE imaging sequence, the polyepoxyamine resin (B) layer is perfectly integrated with the surface.

# Chapter 7: Conclusions

In Phase 1 of this Kansas Department of Transportation (KDOT) funded research endeavor, the Bossmann group at Kansas State University performed the synthesis and characterization of polyurethane resins from VORANOL 220-110 (DOW) and mixtures of TDI (toluene, diisocyanates) and MDI (methylene diphenyl diisocyanate), as well as polyepoxy/amine resins derived from D.E.R. 332 (Olin Corporation) and diethylenetriamine.

Phase 2 of this research endeavor saw the synthesis and characterization of polyisocyanate/polyepoxyamine co-resins from previously optimized polyisocyanate and polyepoxyamine resins. Improved thresholds of thermal decomposition were observed by means of differential thermogravimetry (DTA) for all synthesized co-resins. The maximum of thermal stability occurred at 395 °C and was observed at a mixing ratio of 75% polyisocyanate and 25% polyepoxyamine resin precursors and 60 minutes of reaction at 25 °C.

In order to discern the chemical reasons for the observed synergy, $^1$H-NMR experiments were conducted, in which two types of cross-reactions between polyisocyanate and polyepoxyamine resin precursors were identified: the formation of an ether-bond by means of an epoxide ring-opening reaction, and the formation of a urea-type bond between a primary amine and an isocyanate. These urea-type bonds are most likely responsible for the observed increase in thermal stability.

The Bossmann group then performed the atomic force microscopy (AFM) and magnetic resonance imaging (MRI) characterization of coated and uncoated concrete wafers that were provided by KDOT in Phase 3 of this project. Reactive coating was performed with a polyisocyanate resin (A) and a polyepoxyamine resin (B). The use of polyisocyanate/ polyepoxyamine co-resins was abandoned, despite their superior thermal stability, because they did not adhere smoothly to concrete wafers surfaces.

It was established by AFM that Type 1 concrete wafers by KDOT have a surface roughness of ± 100 nm, which must be regarded as very smooth. Type 2 concrete wafers that were made from cement paste feature a significantly larger surface roughness (± 1000 nm). Both polyisocyanate model resin (A) and the polyepoxide model resin (B) were able to significantly smooth the Type 2

wafers' surfaces. Polyepoxide model resin (B) performed better than polyisocyanate model resin (A).

MRI characterization of both wafer types indicated the presence of air and water bubbles, which are more pronounced in Type 2 wafers. Type 1 wafers show an inferior MRI signal-to-noise-ratio, most likely due to the presence of paramagnetic cations in the material.

Coating of Type 2 wafers with both polyisocyanate model resin (A) and the polyepoxide model resin (B) led to smoothly coated surfaces, in agreement with the AFM findings. Polyepoxide model resin (B) performed better than polyisocyanate model resin (A). In both types of coated wafers, air and—more importantly—water bubbles were present below the coatings. It is assumed that they were already present in the wafers. It would be desirable to study the chemical binding of Resin (A) and Resin (B) in wafers that do not exhibit these structural defects. This would provide enhanced insight into the binding mechanisms of Resins (A) and (B) to concrete.

FLASH, RARE, and Turbo-RARE imaging clearly demonstrate that polyepoxyamine resin (B) is a very suitable polymer coating for Type 2 concrete wafers. This proves that ultra-high-field MRI imaging is an excellent method for imaging polymer-concrete interfaces. The results clearly demonstrate that polyepoxyamine resins are superior as protective concrete coatings to polyurethane coatings, which were found not to be strongly adhesive. Mixtures of polyepoxyamine and polyurethane resins were dominated by their polyurethane content and are not as suitable as pure polyepoxyamine resins. Polyepoxyamine resin (B) was found to behave optimally on Type 2 concrete wafers, which are an excellent model system for concrete used in the transportation sector.

# References

Akindoyo, J. O., Beg, M. D. H., Ghazali, S., Islam, M. R., Jeyaratnam, N., & Yuvarajc, A. R. (2016). Polyurethane types, synthesis and applications – a review. *RSC Advances, 6*(115), 114453-114482.

Hara, O. (1990, December 20). Curing agents for epoxy resin. *Three Bond Technical News, 32*, 1–10.

Harada, M., Sumitomo, K., Nishimoto, Y., & Ochi, M. (2009). Relationship between fracture toughness and domain size of liquid-crystalline epoxy resins having polydomain structure. *Journal of Polymer Science, Part B: Polymer Physics, 47*(2), 156–165.

Heidemann, R. M., Seiberlich, N., Griswold, M. A., Wohlfarth, K., Krueger, G., & Jakob, P. M. (2006). Perspectives and limitations of parallel MR imaging at high field strengths. *Neuroimaging Clinics of North America, 16*(2), 311–320, xi.

Olin Corporation. (2019a). *Curing agents and hardeners*. Retrieved from https://olinepoxy.com/products/curing-agents-and-hardeners/

Olin Corporation. (2019b). *Liquid epoxy resins*. Retrieved from https://olinepoxy.com/products/liquid-epoxy-resins/

Ratna, D. (2003). Modification of epoxy resins for improvement of adhesion: a critical review. *Journal of Adhesion Science and Technology, 17*(12), 1655–1668.

Tang, M.-Y., Zhang, X.-M., Chen, T.-W., & Huang, X.-H. (2015). Various diffusion magnetic resonance imaging techniques for pancreatic cancer. *World Journal of Radiology, 7*(12), 424–437.

Yamamoto, M., Nishikawa, N., Mayama, H., Nonomura, Y., Yokojima, S., Nakamura, S., & Uchida, K. (2015). Theoretical explanation of the lotus effect: Superhydrophobic property changes by removal of nanostructures from the surface of a lotus leaf. *Langmuir, 31*(26), 7355–7363.